Therapeutic strategies for the treatment of colorectal cancer using FXR signaling and one carbon metabolism

Minki Kim

The Graduate School
Yonsei University
Department of Medical Science

Therapeutic strategies for the treatment of colorectal cancer using FXR signaling and one carbon metabolism

A Dissertation Submitted
to the Department of Medical Science
and the Graduate School of Yonsei University
in partial fulfillment of the
requirements for the degree of
Doctor of Philosophy in Medical Science

Minki Kim

June 2024

This certifies that the Dissertation of Minki Kim is approved.

Thesis Supervisor Sungsoon Fang

Thesis Committee Member Ki Taek Nam

Thesis Committee Member Hosung Jung

Thesis Committee Member Eun Jung Park

Thesis Committee Member Hyunkyung Kim

The Graduate School
Yonsei University
June 2024

ACKNOWLEDGEMENTS

First, I want to convey my profound appreciation to Professor Sungsoon Fang, my advisor, for providing steadfast support, guidance, and encouragement during the entire duration of my research. Their expertise and dedication to excellence have consistently inspired my work.

I also express gratitude to the individuals on my thesis committee, Professor Ki Task Nam, Professor Hosung Jung, Professor Eun Jung Park, and Professor Hyunkyung Kim. Their valuable insights and constructive feedback have greatly enhanced the caliber of my research.

I would like to express my gratitude to the colleagues in my lab who shared this journey with me during my degree. Dr. Hyeonhui Kim, Dr. Yeseong Hwang, Dr. Nahee Hwang, Jae Woong Jeong, Sugyeong Jo, Seyeon Joo, Chae Min Lee, and Ye-Chan Park played a crucial role in steering my research in the right direction through their insightful discussions. And, especially, Ph.D. candidate Seyeon Joo helped me with many experimental aspects.

Finally, I want to convey my heartfelt appreciation to my parents for their unwavering love and support.

TABLE OF CONTENTS

LIST OF FIGURES

LIST OF TABLES

ABSTRACT

Therapeutic strategies for the treatment of colorectal cancer using FXR signaling and one carbon metabolism

Colorectal cancer (CRC) is one of the common tumors with a poor prognosis. Several studies have shown that continous administration of bile acids is carcinogenic and that CRC is correlated with the expression of farnesoid X receptors (FXR), a superfamily of nuclear receptors. Deficiency of the FXR is found in CRC, suggesting that restoration of FXR is the approach to treating CRC. However, FXR activation induced down regulation of proliferation but not cell death. I hypothesized that cells with activated FXR have a compensatory survival pathway. To investigate the survival pathway, I performed mRNA and single-nucleus RNA sequencing data analysis and found that activation of FXR increased the one-carbon metabolism pathway. Activating FXR activates ATF4, which is a transcription factor for one-carbon metabolism genes, and found that activated FXR co-binding with ATF4 increases the transcriptional activity of ATF4. Next, I observed that the activation of FXR combined with the inhibition of one-carbon metabolism had a synergistic effect on reducing proliferation in CRC. Collectively, my data demonstrate that inhibiting one-carbon metabolism augments the anti-tumor effect mediated by FXR in CRC.

Key words : colorectal cancer; FXR; one-carbon metabolism

1. INTRODUCTION

Colorectal cancer (CRC) is the third most common type of cancer, associated with high rates of mortality and morbidity globally. The risk factors for CRC include obesity, diabetes, a high-fat diet, inflammatory bowel disease, and increased bile acid levels.[1-3] Most cases of CRC occur sporadically, whereas others are caused by mutations in various genes.[4] Dysregulated activation of the Wnt and RAS pathways is significant in the development of CRC at the cellular level.[5-7] Mutations in key genes associated with these pathways, such as adenomatous polyposis coli (APC) and KRAS, are common in human CRC, contributing to the initiation and progression of tumorigenesis. The APC gene is categorized as a tumor suppressor gene and encodes a protein crucial for regulating DNA replication and cell division.

CRC progresses through three mechanisms: chromosomal instability (CIN), microsatellite instability (MSI), and the CpG island methylator phenotype (CIMP). Mutations in KRAS and BRAF are mutually exclusive but both lead to the upregulation of the RAS/RAF/MAPK signaling pathway, playing a critical role in CRC development. KRAS encodes a protein that binds guanosine triphosphate (GTP)/guanosine diphosphate (GDP), and mutations in KRAS are found in approximately 30~40% of CRCs. While KRAS mutations are widely recognized as predictive markers for resistance to epidermal growth factor receptor targeted antibodies in metastatic CRC, their prognostic significance is still debated.

Bile acids, which are metabolites of cholesterol synthesized in the liver, play a crucial role in lipid metabolism by promoting the absorption of fat and fat-soluble vitamins in the intestine. The traditional synthesis of bile acids begins with cholesterol 7α-hydroxylase (CYP7A1), producing cholic acid (CA) and chenodeoxycholic acid (CDCA) as primary bile acids. Once excreted into the intestine via the biliary system, gut microbiota facilitate the deconjugation and transformation of these primary bile acids into secondary bile acids, such as deoxycholic acid (DCA) and lithocholic acid (LCA). These bile acids are reabsorbed from the colon through the circulation for reuse.[8,9]

Multiple studies have demonstrated that prolonged exposure to elevated levels of bile acids has carcinogenic effects, particularly in the context of CRC. Research on human studies and mouse models of intestinal cancer indicates a significant association between elevated bile acid levels and

an increased occurrence of CRC.[10,11] Although various pathways have been suggested to explain the tumor-promoting activity of bile acids during the post-initiation phase of intestinal tumorigenesis, the precise mechanisms remain unclear.

The farnesoid X receptor (FXR), belonging to the nuclear receptor superfamily and recognized as a bile acid receptor, functions as a transcription factor pivotal in regulation bile acid homeostasis in liver.[12,13] FXR exists in four distinct isoforms. FXR includes several distinct regions such as the N-terminal activation function 1 (AF-1) domain, the DNA binding domain (DBD), the ligand binding domain (LBD), the C-terminal ligand-dependent activation function 2 (AF-2) domain, and a hinge region (H) that serves as a flexible link between the DBD and LBD. While the specific functions of the AF-1 domain in FXR remain unclear, in other nuclear receptors (NRs), the AF-1 domain is structurally variable and more prone to post-translational modifications. The sole evidence of the AF-1 domain's function in FXR to date is its interaction with beta-catenin, which attenuates the formation of the beta-catenin/TCF4 complex upon ligand binding. FXR isoforms form dimers with the Retinoid X receptor (RXR) and attach to two specific FXR response elements (FXRE), which are the inverted hexamer spaced by one nucleotide (IR-1) motif and the everted hexamer repeat spaced by two nucleotides (ER-2) motif, thereby regulating the transcriptional activity of target genes.

FXR is the main detector for bile acid levels. Bile acids directly bind to the LBD of FXR, affecting its function to activate or repress transcription. As a receptor for bile acid, FXR is primarily expressed in tissues regularly exposed to bile acids, such as liver, intestine, and kidneys. Recent clinical trials have explored FXR agonist compounds for conditions such as cholestasis and nonalcoholic steatohepatitis (NASH). These compounds are also under investigation as a prospective treatment strategy for CRC, given their association with the disease.[14]

Although numerous studies have established a link between FXR and CRC, the precise underlying mechanisms remain elusive. Recent observations highlight the inhibition of intestinal stem cell proliferation and cancer progression upon FXR activation. These results indicated positioning FXR as a therapeutic agent for CRC.[15-17] Notably, activation of FXR alone does not induce complete cancer cell death, suggesting the existence of an unknown pathway sustaining CRC survival.

One-carbon metabolism regulates many biochemical pathways, including redox balance,

epigenetic regulation, biosynthesis, and homeostasis of amino acids such as serine and glycine.[18] Cells generate one-carbon units through various pathways, including the conversion of serine to glycine, the glycine cleavage system (GCS), and the metabolism of other amino acids. The enzymes serine hydroxymethyltransferase-1(SHMT1) and serine hydroxymethyltransferase-2(SHMT2) catalyze the conversion of serine to glycine. In this reaction, the one-carbon unit cleaved from serine and transferred to THF, resulting in the formation of methylene-THF.

One-carbon units are utilized in two biological pathways, the methionine cycle and the folate cycle. Folates are adaptable methyl donors that carry and chemically activate one-carbon units. Because animals can't internally synthesize folates, they must obtain them entirely from dietary sources. Methionine is transformed into S-adenosylmethionine (SAM) by methionine adenosyltransferase, serving as a universal donor. In methyl transfer reactions, SAM changes into S-adenosylhomocysteine (SAH), which then undergoes hydrolysis to produce homocysteine (HCY) and adenosine, thus completing the methionine cycle.

One-carbon units are crucial for synthesizing both purine and pyrimidine nucleotides, essential building blocks for DNA and RNA synthesis. Due to cancer cells high proliferation rate and the requirement of nucleotides, cancer cells require a significant supply of one-carbon units for nucleotide synthesis. Although tumors frequently show altered patterns of DNA methylation. DNA methylation is critical for the regulating gene expression, and in cancer, hypermethylation of tumor-suppressor gene promoter regions can lead to reduced expression of genes. Additionally, NADH and NADPH are crucial cofactors that provide electrons for redox balance, generated through one-carbon metabolism and essential in various pathways.

The production of serine and glycine, along with the process of one-carbon metabolism, plays critical roles in supporting the survival and rapid growth of cancer cells by providing essential building blocks such as proteins, nucleic acid, and lipids.[19] Moreover, the compartmentalization of one-carbon metabolism inside the mitochondria, orchestrated by SHMT2, signifies a specific adaptation in chemotherapy-resistant cells. The sensitivity of CRC to chemotherapy is influenced by alterations in serine metabolism.[20] These findings suggest that targeting one-carbon metabolism could be a viable therapeutic strategy.

Herein, I outline the pivotal role of one-carbon metabolism in the activated FXR-mediated survival pathway in CRC. I observed an upregulation of one-carbon metabolism upon FXR

activation. Furthermore, I found that the activated FXR, acting as a nuclear receptor and transcription factor, binds to ATF4, leading to an increase in ATF4 transcriptional activity and recruitment. These findings indicate that activated FXR plays an additional role in the process. In addition, I found that combination treatment with an FXR agonist and one-carbon metabolism inhibitor significantly reduced cancer growth. My findings suggest that the inhibition of one-carbon metabolism potentiates the anti-tumor effects of FXRs in CRC.

2. MATERIALS AND METHODS

2.1. Cell culture

CRC cell lines (DLD1, HCT15, HT29, LoVo, SW620, and SW480) were obtained from the American Type Culture Collection (ATCC) and the Korean Cell Line Bank (KCLB). Cell lines were grown in RPMI-1640 (Corning, 10-041-CV) culture media supplemented with 10% (v/v) fetal bovine serum (FBS; Corning, 35-015-CV) and 1% penicillin-streptomycin (PS; Gibco, 15140122) at 37℃ in humidified atmosphere with 5% carbon dioxide (CO2).

2.2. Western blot assay

Protein sample was extracted from cells using EBC200 lysis buffer (200 mM NaCl, pH 8.0; 50 mM Tris-HCl; NP-40 0.4%) supplemented with 0.5M EDTA, protease inhibitor (GenDEPOT, #P3100), and phosphatase inhibitor (GenDEPOT, #P3200). Proteins were quantified using a bicinchoninic acid assay (BCA; Thermo Scientific, #23225). Subsequently, 20 ug of proteins were placed onto SDS-PAGE gels and then transferred to PVDF membranes. The membrane was blocked in 5% skim milk for 1 h, and then incubated at 4℃ over-night with diluted antibodies (ATF4; Cell Signaling #11815, β-actin; Santa Cruz #sc-47778, CCNB1; Santa Cruz #sc-245, CCNE1; Santa Cruz # sc-247, CDK2; Abcam # ab32147, PHGDH; Santa Cruz #sc-100317, PSAT1; Proteintech #10501-1-AP, SHMT2; Santa Cruz #sc-390641, MTHFD2; Cell Signaling #98116S). The membranes were washed using TBST (Tris-buffered saline containing 0.1% Tween20), and incubated for 1 h at room temperature(RT) with horseradish peroxidase-conjugated anti-mouse (Cell Signaling, #7076S) or anti-rabbit (Abcam, #ab6721) antibodies. Bound antibody signals were detected using Clarity Western ECL substrates (#1705061 and #1705062; Bio-Rad).

2.3. RNA extraction and Real-time quantitative PCR analysis

Total RNA was isolated from the cells using TRIzol reagent (Invitrogen, #15596018). cDNA was synthesized from 1 ug of total RNA using ImProm-II™ Reverse Transcriptase (Promega, #A3803) according to the manufacturer's instructions. qPCR (real-time PCR) was performed using TOPreal 2X PreMIX (SYBR Green; Enzynomics, #RT501M) and specific primers on a CFX

Connect Real-Time PCR instrument (Bio-Rad, #1855201). Gene expression results were normalized to the 36B4 mRNA expression levels. The nucleotide sequences of the primers are in Table 1.

2.4. Cell proliferation assay

CRC cells (5×103 cells/well) were seeded in 96-well and 48-well plates for proliferation and viability assays. More than three wells were seeded for each experimental state. GW4064 (MCE, #HY-50108), fexaramine (Santa Cruz, #sc-203580), NCT-503 (Selleckem, #s8619), and SHIN-1 (MCE, #HY-112066) were dissolved in DMSO. Cell Counting Kit-8 (CCK-8; Dojindo, #CK04) and MTT (Thermo Fisher Scientific, #M6494) were used to assay cell proliferation and viability. After the cells were incubated with chemicals for 24 h, 10 μl of the CCK-8 or 0.3 μg of the MTT solution was added to each well, followed by incubation for 1 h or 2 h (1 h for CCK-8, 2 h for MTT). The absorbance was measured at 450 nm (CCK-8) and 570 nm (MTT) using a microplate absorbance reader (Thermo Fisher Scientific, #51119300) to calculate the cell proliferation rate.

2.5. Measurement of ROS content

ROS levels were measured using DCFDA (Invitrogen, #D399). HT29 cells were plated and treated with DMSO, Fexaramine, GW4064, NCT-503, SHIN-1, or combination for 24 h. After incubation, with DCFDA for 30 min at 37°C, the fluorescence intensity of the plates was assayed using a Varioskan Flash 3001 fluorometer (Thermo Fisher Scientific).

2.6. Measurement of GSH content

To measure the total GSH content, CRC cells (DLD1, HT29) were stained with mBBr (10 μM) for 10 min in a 37 °C incubator. Fluorescence intensity was measured within 30 min using flow cytometry (FACSVerse, BD Biosciences), and the data were subsequently analyzed using FlowJo software (version 10.4.2).

2.7. Measurement of NADPH level

The level of NAPDH was measured using an NADP/NADPH quantitation kit (Sigma, #MAK038-

1KT), and absorbance was measured using a microplate absorbance reader (Thermo Fisher Scientific, #51119300).

2.8. Cell cycle assay

CRC cells (DLD1 and HT29) were seeded in six well plates and treated with an FXR agonist (fexaramine) for 24 h. The cells were harvested and washed with PBS. After washing, the cells were incubated with PBS containing 30 ug/ml of propidium iodide, 0.2 mg/ml of RNase A, and 0.1% Triton X-100 for 15 min in a 37 °C incubator. Cell cycle progression was measured using flow cytometry (FACSVerse, BD Biosciences), and the data were analyzed using FlowJo software (version 10.4.2).

2.9. Co-Immunoprecipitation

Endo Co-IP and Co-IP overexpression assays were performed according to standard procedures. Endo Co-IP were plated for HT29 cells and lysed in EBC200 lysis buffer. Overexpression of Co-IP was performed in HEK293T cells, which were transfected with ATF4-GFP and FXR-Flag plasmids overnight. Proteins were incubated with ATF4, FXR (Thermo Fisher Scientific, #417200), GFP (Santa Cruz, #sc-9996), and FLAG (Sigma, #F3165) primary antibodies. The samples were incubated overnight at 4℃ rotator. After incubation, protein A/G agarose beads were added and incubated at 4℃ rotator for 2 h. The beads were washed at least four times, and cleared beads were obtained. The sampled beads were subjected to SDS-PAGE followed by Western blot analysis.

2.10. shRNA stable cell line generation

shRNAs targeting ATF4 (TRCN0000013574, TRCN0000013575) were purchased from the Yonsei System Biology Core TRC shRNA service. The pMD2.G, psPAX2, and pLKO.1 shRNA vectors were transfected into HEK293T cells using FuGENE HD transfection reagent (Promega, #E2311) according to the manufacturer’s protocol to produce lentiviruses. HT29 cells were transduced with the viral supernatant and selected using puromycin.

2.11. siRNA knockdown

The siRNAs (ATF4, #sc-35112; control A, #sc-37007) used in the study were purchased from Santa Cruz Biotechnology. Lipofectamine RNAiMAX (Invitrogen, #13778150) was used to transfect HT29 cells with 50 nM siRNA following the manufacturer's protocol.

2.12. RNA sequencing analysis

RNA was isolated from each sample using TRIzol reagent following the manufacturer's instructions. Libraries were constructed by Macrogen (Seoul, Korea, www.marcogen.com) using Tru-Seq Stranded mRNA (Illumina) according to the manufacturer's protocol, and sequencing was performed using the NovaSeq 6000 system. The raw sequence was qualified using FastQC (0.11.7 version), low quality sequences were removed using Trimmomatic (0.38 version), and sequences were mapped using the HISAT2 program (2.1.0 version). Assembly and annotation were performed using the StringTie (1.3.4d version). The DEGs were evaluated using edgeR.

2.13. single-nucleus RNA sequencing analysis

Organoid nuclei were isolated by flow cytometry. We used the 10X Genomics Chromium Instrument and cDNA synthesis kit (Chromium Next GEM Automated Single Cell 3′ Library and Gel Bead Kit v3.1) to produce a barcoded cDNA library for single nuclei RNA-sequencing. Library quality was confirmed using an Agilent Bioanalyzer, and two paired-end 100bp Flow Cells on a Novaseq 6000. The Fastq files were demultiplexed and aligned to the human genome using the 10X Genomics Cell Ranger. The CellRanger results were loaded into R using the read10X package in Seurat. The Seurat package was used to determine gene expression and clusters. Before quality control, contamination and filtered droplets were quantified experimentally using the Debris Identification and Expectation Maximization package. Quality control of data was filtered with the following cutoff values: number of genes per cell (nFeature) between 200 and 7500, whole number of read counts (nCount) below 30000, and percentage of mitochondria (percent_MT) lower than 5%. To conduct normalization, dimensionality, reduction, clustering, and differential expression analyses, we employed the Seurat package, as mentioned above. To perform an integrated analysis of the dataset, we utilized the FindIntegrationAnchors and IntegrateData commands, also known as canonical correlation analysis (CCA). During the clustering process, we used the FindClusters function, which was segmented at a resolution of 0.4. To analyze the cell populations with restored

expression, we employed an expression recovery algorithm known as ALRA. GSEA and GO enrichment analyses of the marker genes were performed using the escape R package. The scvelo, velocyto, and slingshot packages were used to quantify unspliced and spliced abundances and explore cell trajectories.

2.14. ATAC sequencing analysis

The ATAC-seq samples were duplicated, and processing was performed using Macrogen. The number of cells was determined using a LUNA-FL Automated Fluorescence Cell Counter (Logos Biosystems). Subsequently, the concentration of nuclei was quantified following cell lysis using the Countess II Automated Cell Counter (Thermo) and their morphology was examined. The libraries were PCR amplified and quantified using qPCR (KAPA Library Quant Kit). The HiSeq platform system (Illunina) was used to sequence the libraries. The sequence was qualified using FastQC (0.11.7 version), trimmed with Trim Galore (0.5.0 version), and aligned using Bowtie2 (2.3.5.1 version). Peaks were called from the alignment BAM files using MACS2 (2.1.1 version). Peaks that overlapped with the regions blacklisted by ENCODE were excluded from the analysis. ChIPseeker (1.16.1 version) supported the annotation of peaks and provided chromosome coverage.

2.15. Chromatin immunoprecipitation assay

For ChIP experiments, cells were cross-linked for 5 min at room temperature by the addition of 1% (w/v) methanol-free formaldehyde (Thermo, #28908), followed by the inhibition cross-linking with 0.125 M glycine. The cells were collected using cell lysis buffer (150 mM NaCl, pH 7.8 50 mM Tris-HCl, 0.5% NP-40, 1% Triton X-100, pH 7.6 5 mM EDTA, and 1X protease inhibitor) after washing with cold PBS. The cells were mechanically broken by passing through a 1 ml insulin syringe, followed by centrifuging at 12000 g for 1 min at 4℃. A Covaris ultrasonicator (#M220) was used to perform chromatin shearing on a pellet re-suspended in shearing buffer (1% SDS, pH 7.6 10 mM EDTA, pH 8.0 50 mM Tris-HCl, and 1X protease inhibitor). The samples diluted by dilution buffer (150 mM NaCl, pH 8.0 20 mM Tris-HCl, pH 7.6 2 mM EDTA, 1% Triton X-100, and 1X protease inhibitor), immunoprecipitated using ATF4, FXR, acetyl histone H3 (Millipore, #06-599), and rabbit IgG control antibody (Cell Signaling, #2729), and incubated with protein A/G agarose beads for 1 h at 4℃. Subsequently, washes were performed with buffer 1 (150 mM NaCl,

pH 8.0 20 mM Tris-HCl, pH 7.6 2 mM EDTA, 0.1 % SDS, and 1 % Triton X-100), buffer 2 (500 mM NaCl, pH 8.0 20 mM Tris-HCl, pH 7.6 2 mM EDTA, 0.1 SDS, and 1 % Triton X-100), buffer 3 (0.25 M LiCl, pH 8.0 10 mM Tris-HCl, pH 7.6 1 mM EDTA, 1 % NP-40, and 1 % deoxycholate), and TE buffer (pH 8.0 10 mM Tris-HCl, pH 7.6 1 mM EDTA) three times. The protein–chromatin complexes were incubated at 65℃ overnight to reverse crosslinking, followed by incubation with proteinase K to digest the protein. DNA was purified using a QiAquick PCR purification kit (Qiagen, #28106) and analyzed by qPCR using the following primers: PSAT1-F ; 5'-AGGAGCAACTGCTTCGACTC-3', PSAT1-R ; 5'- CCTGCGCTAATTGGTTCGC-3'.

2.16. Chromatin immunoprecipitation sequencing analysis

ChIP-seq analysis of ATF4 and GW4064 expression in HT29 cells was done. Samples were prepared using a ChIP assay. The quality and quantity of DNA were evaluated using Quant-IT PicoGreen (Invitrogen) and an Agilent High Sensitivity DNA Kit on an Agilent 2100 Bioanalyzer (Agilent Technologies). The TruSeq ChIP Sample Preparation Kit (Illumina) was used to prepare libraries according to the manufacturer's instructions. Finally, the indexed libraries were sequenced with the HiSeqX™ platform (Illumina) by Macrogen Incorporated.

2.17. IHC staining

After the samples were deparaffinized and rehydrated, sections for ATF4, PSAT1, and SHMT2 staining were placed in FLEX Target solution (DAKO) for antigen retrieval by boiling in a PT link for 20 min at 95 °C. To deactivate the endogenous peroxidase, sections were exposed to 3% H2O2 for 10 min and then rinsed with TBS for 5 min, twice. Subsequently, the slides were incubated for 1 h with a 1:300 dilution against ATF4 and (1:100 dilution), PSAT1, and SHMT2 antibodies at room temperature. Following three 5-min washes with TBS, the slides were incubated with a secondary antibody (DAKO, K4003) for 20 min at room temperature. Diaminobenzidine (DAB) (DAKO, K3468) was utilized for a 5-min color development. Finally, the slides were counterstained with hematoxylin for 10 min, followed by dehydration and mounting.

2.18. Immunocytochemistry (ICC)

CRC cells were fixed in 4% paraformaldehyde for 30 min at room temperature. The cells were

exposed to primary antibodies overnight at 4℃, followed by treatment with Alexa Fluor 488- and 546-conjugated secondary antibodies for 1 h, with Hoechst staining serving as a nuclear counterstain. All the above operations between different reagents were washed three times with PBS. The antibodies used were as follows: ATF4 (Cell Signaling Technology, #11815) and anti-FXR (Thermo Fisher Scientific, #417200).

2.19. Dual Luciferase reporter assay

293T cells were plated in 24-well dishes at 50% confluence. After 24 h, for each well, different plasmids (β-Galactosidase vector, pGL3-CHOP promoter-luc vector, CMV10-ATF4-GFP vector, and CMV10-FXR-Flag vector) were transfected using PEI (polyethylenimine). After 24 h, the cell plates were harvested and lysed. Luciferase reported activity was measured using the Dual-Luciferase assay using luciferase assay buffer (D-luciferin [Duchefa biochemie, #L1349], KPO4 [pH 7.8], MgCl2, and ATP [pH 7.0]) β-Galactosidase assay buffer (phosphate buffer, MgCl2, and ONPG), and a microplate luminometer (EG&G Berthold).

2.20. Animal studies

All mouse xenograft studies were approved by the Institutional Animal Care and Use Committee of Yonsei University College of Medicine and followed the relevant guidelines. The puromycin-resistant HT29-mCherry cell line was generated from media containing a lentivirus produced by co-transfecting pLL-mCherry-puro, pMD2.G, and psPAX2 in 293T cells. HT29-mCherry cells (5 × 106) were subcutaneously injected into the flank of nude mice. When the xenograft mouse tumors were established, GW4064 (20 mg/kg), NCT-503 (30 mg/kg) and SHIN1 (30 mg/kg), as single chemicals and in combination, were injected intraperitoneally twice a week (GW4064) and three times a week (NCT-503, SHIN1) for 3 weeks. The tumor volume was measured and recorded using an in vivo optical imaging system (IVIS).

2.21. Spatial analysis

The spatial dataset was available from a spatial transcriptomics research website (http://www.cancerdiversity.asia/scCRLM/). We employed the R and Seurat package, following the 'Analysis of Image-based Spatial Data in Seurat' guide provided by satijalab. In summary, the dataset

and high-resolution image files were imported into R and subjected to normalization using SCTtransform. The normalized data underwent integration and followed the standard workflow for single-cell RNA sequencing, including ScaleData, RunPCA, and RunUMAP. Visualizations of the SCTtransform normalized data were depicted through VlnPlot and SpatialFeaturePlot.

2.22. Statistical analysis

Data are expressed as the mean ± SEM, SD of three independent experiments. The two data sets were compared using the unpaired Student's t-test using GraphPad Prism 9 software. A p value of less than 0.05 was considered to be statistically significant. Differences among three or more groups were assessed using one-way ANOVA, followed by TurkeyHSD test. The mathematical formula used to calculate drug synergy was obtained from SynergyFinder using the HSA model.

Table 1. List of qPCR primers

qPCR primers		
Gene	**Forward**	**Reverse**
DDIT3	GGAAACAGAGTGGTCATTCCC	CTGCTTGAGCCGTTCATTCTC
ATF4	CCCTTCACCTTCTTACAACCTC	TGCCCAGCTCTAAACTAAAGGA
ASNS	GGAAGACAGCCCCGATTTACT	AGCACGAACTGTTGTAATGTCA
FXR	GACTTTGGACCATGAAGACCAG	GCCCAGACGGAAGTTTCTTATT
SLC7A5	CCGTGAACTGCTACAGCGT	CTTCCCGATCTGGACGAAGC
CHAC1	GAACCCTGGTTACCTGGGC	CGCAGCAAGTATTCAAGGTTGT
PHGDH	CTGCGGAAAGTGCTCATCAGT	TGGCAGAGCGAACAATAAGGC
PSAT1	ACAGGAGCTTGGTCAGCTAAG	CATGCACCGTCTCATTTGCG
SHMT1	AGGAAAGGAGTGAAAAGTGTGGAT	GACACCAGTGTCGCTCTGGATCTG
SHMT2	ATGTCTATGCCCTATAAGCTCAACCC	GCCGGAAAAGTCGAGCAGT
MTHFD1	AGGATGTGGATGGATTGACTAGC	CCCTTAGGCGTACAAGGAATG
MTHFD2	GATCCTGGTTGGCGAGAATCC	TCTGGAAGAGGCAACTGAACA

3. RESULTS

3.1. One-carbon metabolism pathway is upregulated in colorectal cancer patient data

The one-carbon metabolism pathway exhibits interconnections with several cellular pathways, such as the serine synthesis and the folate cycle (Fig. 1A). Compared with normal tissues, I observed a significant upregulation of genes related to the one-carbon metabolism pathway in CRC patient tissues (Fig. 1B). Immunohistochemistry (IHC) staining revealed that PSAT1 and SHMT2 expression were markedly increased in CRC patients (Fig. 1D). Furthermore, I initially analyzed the expression of one-carbon metabolism genes in the TCGA COAD database. The analysis showed the upregulation of one-carbon genes in tumor patients had a poor prognosis (Fig. 1C, E). I then established spatial transcriptomic data using published CRC research data.[21] The spatial data clusters were annotated based on H&E staining and cell markers, leading to the identification of four distinct morphological regions. (Fig. 2A, B). As observed from the spatial data, genes related to one-carbon metabolism were upregulated in the tumor sections (Fig. 2C, D).

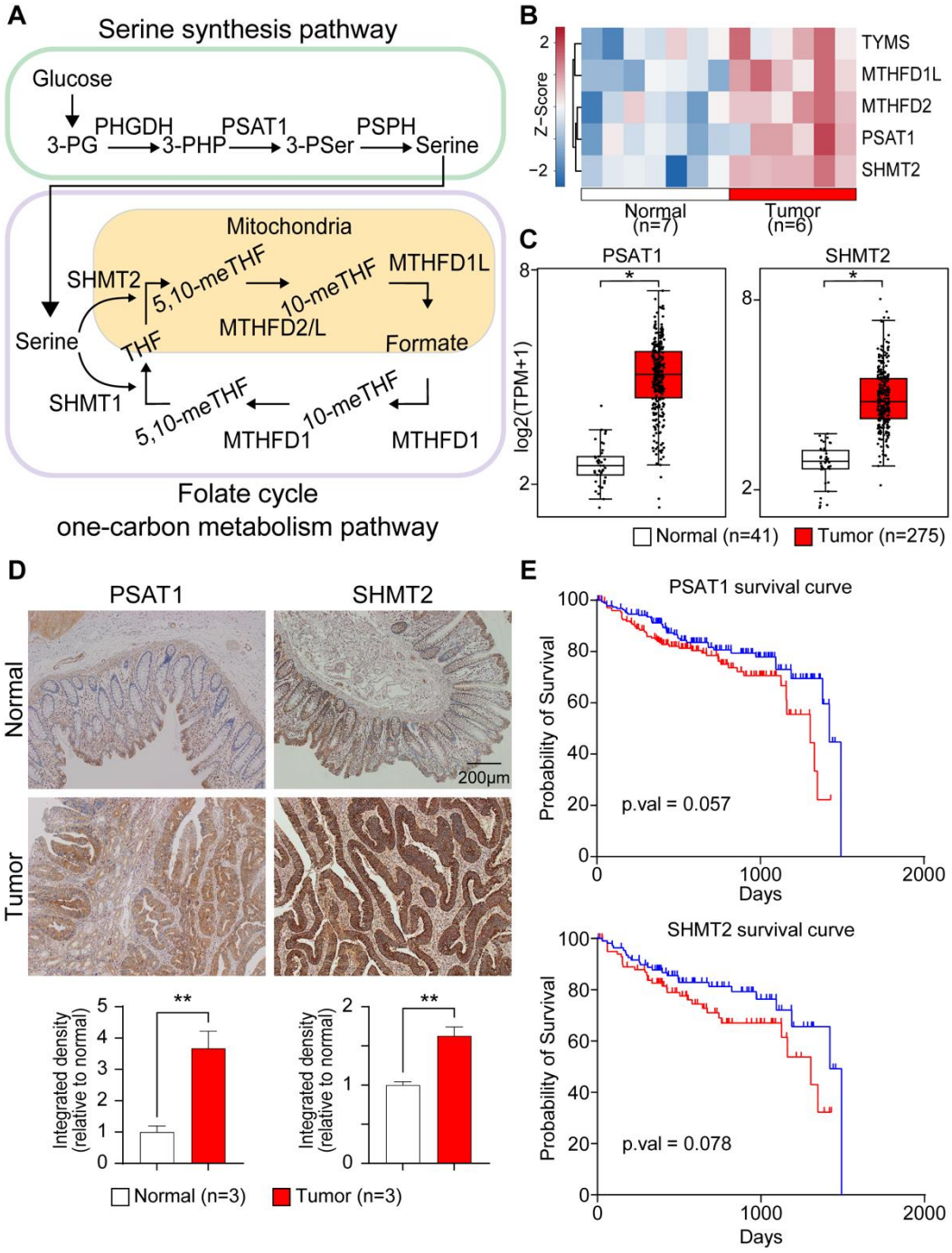

Figure 1. One-carbon metabolism is upregulated in CRC patients. (A) Schematic of one-carbon metabolism. (B) Heat map of mRNA-seq of patients with CRC displaying the expression levels of one-carbon metabolism genes: normal tissue (n=7) and tumor tissue(n=6). (C) Gene expression analysis using GEPIA based on the TCGA database. The boxplot shows PSAT1 and SHMT2 expression in tumor tissues (red, n=275) and normal tissues (white, n=41). (D) IHC staining shows PSAT1 and SHMT2 expression in patients with CRC. Scale bar = 200 μm. (E) Survival curves using Kaplan-Meier analysis based on the TCGA database. The plot shows shorter survival for high expression PSAT1 and SHMT2 patients until 1500 days. Data represent mean + SEM. *$p<0.05$, **$p<0.01$, ***$p<0.001$, ****$p<0.0001$; student's t-test, two tailed.

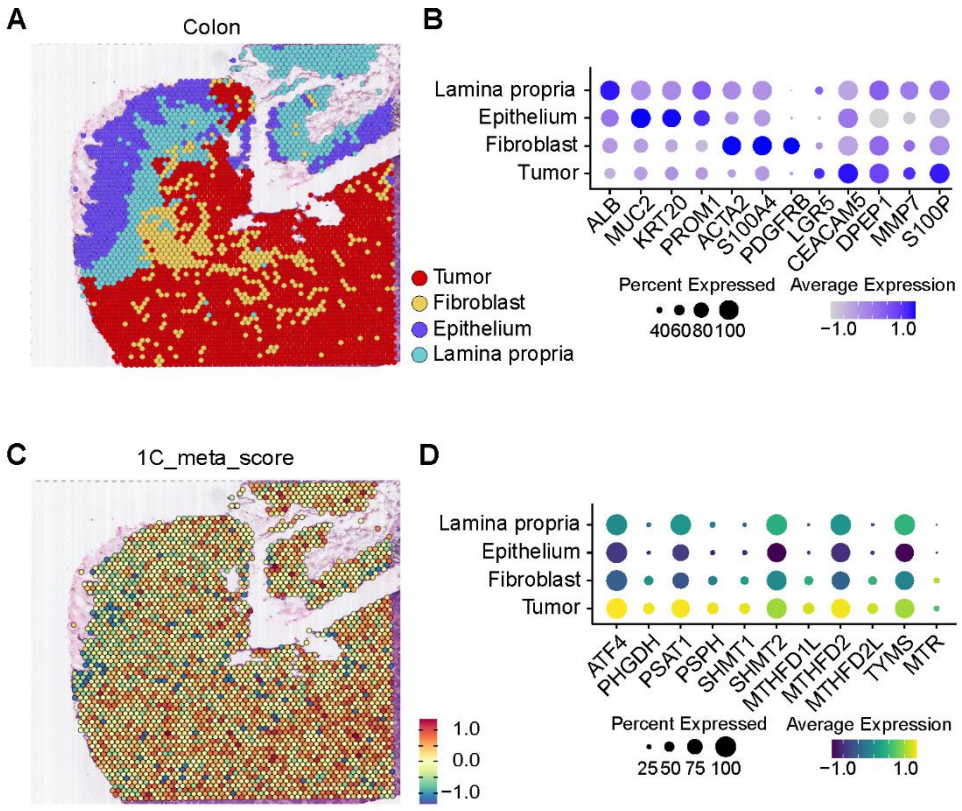

Figure 2. In the spatial data, there is an increase in one-carbon metabolism in the tumor region. (A) The spatial images of unsupervised clustering analysis results. (B) The Dot plot displays the expression levels of cell markers across various morphological regions. (C) Visualization of expression level in one-carbon metabolism genes module. (D) The Dot plot shows the expression level in one-carbon metabolism module genes.

3.2. One-carbon metabolism pathway is increased in cancer regardless of CMS type and mutation of genes

In several studies, the consensus molecular subtype (CMS) is commonly utilized as a classification criterion for CRC.[22] Upon analysis of single-cell sequencing public data, it was observed that while distinctions exist among CMS subtypes, collectively, they exhibit an elevated level of one-carbon metabolism compared to normal samples (Fig. 3A-D). In various studies, the impact of KRAS mutations on the efficacy of epidermal growth factor receptor (EGFR) inhibitors, commonly employed in CRC treatment, has been extensively examined. However, my investigation revealed that the inhibitor targeting the one-carbon metabolism pathway demonstrated a reduction in proliferation comparable to that of anti-EGFR treatment, irrespective of the KRAS mutation status (Fig. 3E). These results suggest that one-carbon metabolism pathway is involved in CRC progression. Also, one-carbon metabolism can be a potential therapeutic strategy in CRC.

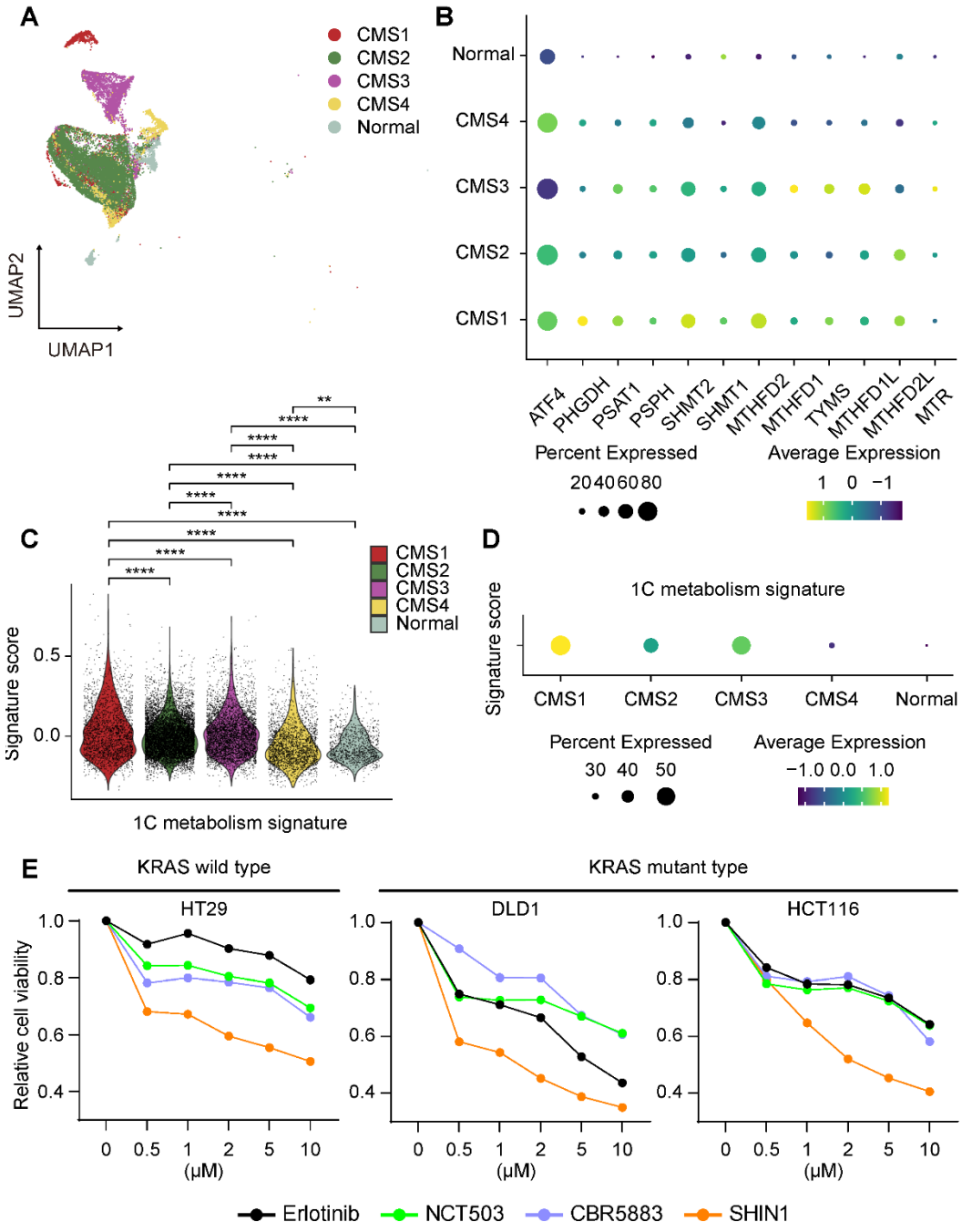

Figure 3. High levels of one-carbon metabolism are observed regardless of CMS or mutation status. (A) UMAP visualization of cells in labeled CMS subtype and normal. (B) The Dot plot shows the expression level in one-carbon metabolism module genes. (C) Visualization of expression level in one-carbon metabolism genes module labeled CMS subtype. (D) The Dot plot shows the expression level in one-carbon metabolism module genes score. (E) Dose-dependent cell viability of the Erlotinib (EGFR inhibitor), NCT-503 (PHGDH inhibitor), CBR-5883 (PHGDH inhibitor), SHIN1 (SHMT2 inhibitor). *p<0.05, **p<0.01, ***p<0.001, ****p<0.0001; student's t-test, two tailed.

3.3. Inhibition of cancer cell proliferation and cell cycle by FXR activation without inducing cell death

Studies have indicated that FXR activation is a potential treatment strategy for patients with CRC. The result showed that fexaramine, FXR agonist, treatment inhibited the proliferation of CRC cell lines (Fig. 4A). After treating the cells with fexaramine, which led to the inhibition of cell proliferation, I analyzed the cell cycle distribution using flow cytometry. The result showed an accumulation of cells in the G0/G1 phase (Fig. 4C). And then, I indicated that the protein levels of genes associated with the cell cycle were also downregulated by the activation of FXR (Fig. 4B). However, I observed that cancer cells do not undergo apoptosis with the activation of FXR (Fig. 4D, E).

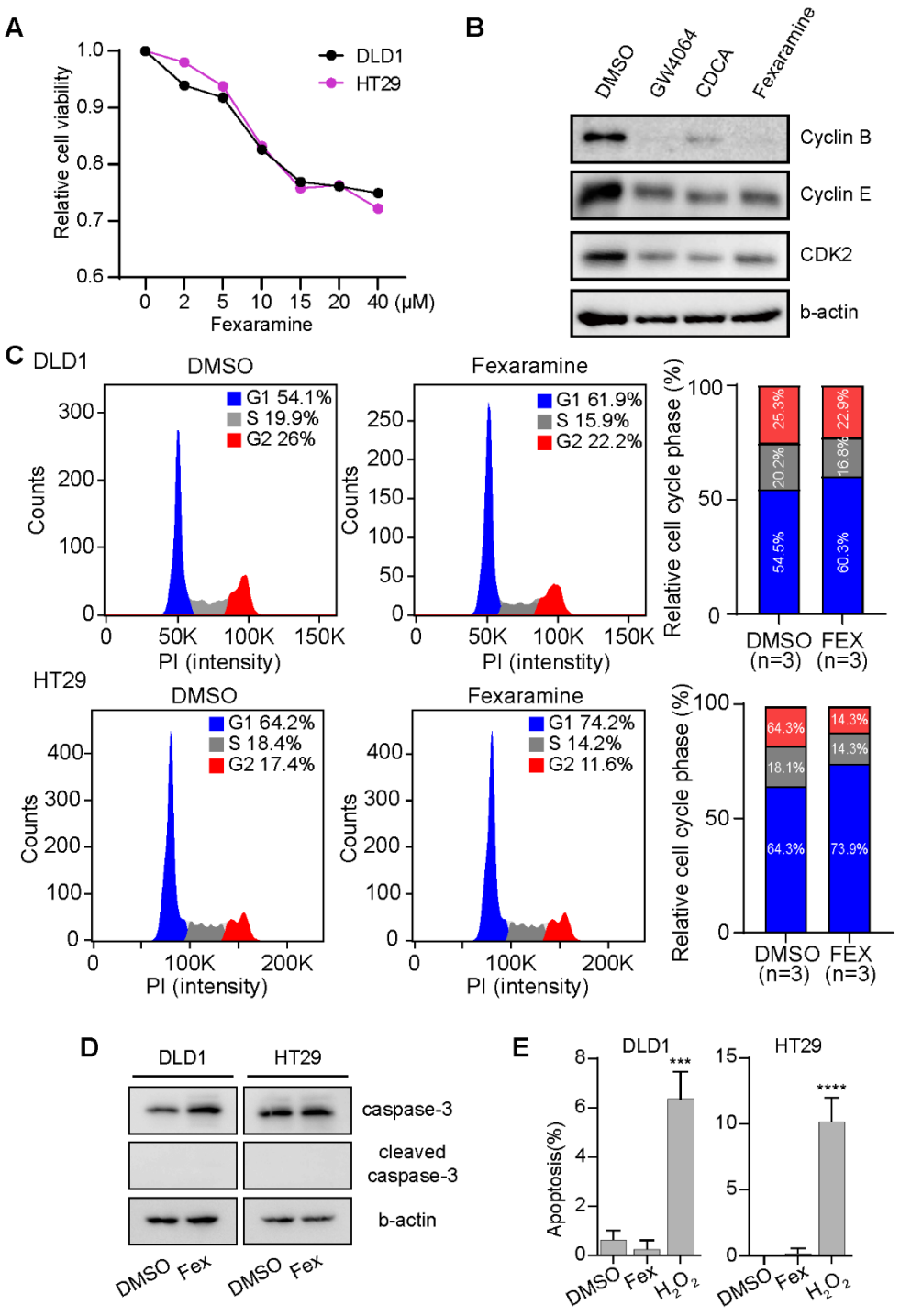

Figure 4. The activation of FXR demonstrates a decrease in proliferation and cell cycle progression. (A) Dose-dependent cell viability of the FXR agonist (Fexaramine) on the growth of two CRC cell lines: DLD1 and HT29. (B) The Western blot shows related genes of cell cycle (cyclin B, cyclin E, CDK2, β-actin) treated with FXR agonist (GW4064, CDCA, fexaramine) for 24h. (C) A colorectal cell (DLD1 and HT29) was treated with fexaramine (15 μM) for 24 h. Cell cycle analysis was conducted using propidium iodide staining in flow cytometry. (D) The Western blot shows Caspase3 and β-actin treated with fexaramine for 24 h. (E) A positive control of H2O2 (10 uM) was employed and selected numbers were used for quantifying the percentage of fragmented nuclei. Data represent mean + SEM. *$p<0.05$, **$p<0.01$, ***$p<0.001$, ****$p<0.0001$; student's t-test, two tailed.

3.4. Activating FXR initiates a one-carbon metabolism pathway gene expression in CRC

Previous data showed that activation of FXR has a compensatory survival pathway in CRC. To examine the changes in various pathway, I performed RNA sequencing analysis on the CRC cell lines with FXR agonists (Fig. 5A). Treatment with and FXR agonist resulted in the activation of several valuable genes providing evidence for how FXR activation promotes the survival of CRC. Candidate heat map clusters were analyzed using an online database. Gene ontology (GO) analysis of the clusters was performed using DAVID. Significant enrichment was observed among the upregulated genes in cluster 1 and 8, particularly in terms of response to unfolded proteins, serine amino acid metabolic processes, and THF interconversion (Fig. 5B). In addition, the gene set enrichment analysis (GSEA) revealed an upregulation in the gene set related to the UPR signaling pathway (Fig. 5C). By confirming the DDIT3 gene, located downstream of the UPR signaling pathway, I observed a significant upregulation in its expression following treatment with an FXR agonist (Fig. 5D). Moreover, FXR activation led to the upregulation of ATF4 target genes (Fig. 5E). However, level of ATF4 does not affected by activation of FXR and FXR target genes expression showed different responsiveness by FXR activation in cell lines (Fig. 5F). I confirmed that the one-carbon metabolism pathway gene expression was upregulated by the activation of the FXR (Fig. 6A). I found that the mitochondrial serine synthesis pathway and folate cycle site gene expression were specifically upregulated by FXR agonists (Fig. 6B-D). This result confirmed the association between FXR activation and the one-carbon metabolic pathway. In addition, I showed that the FXR, which inhibits cell proliferation, upregulates the one-carbon metabolism pathway.

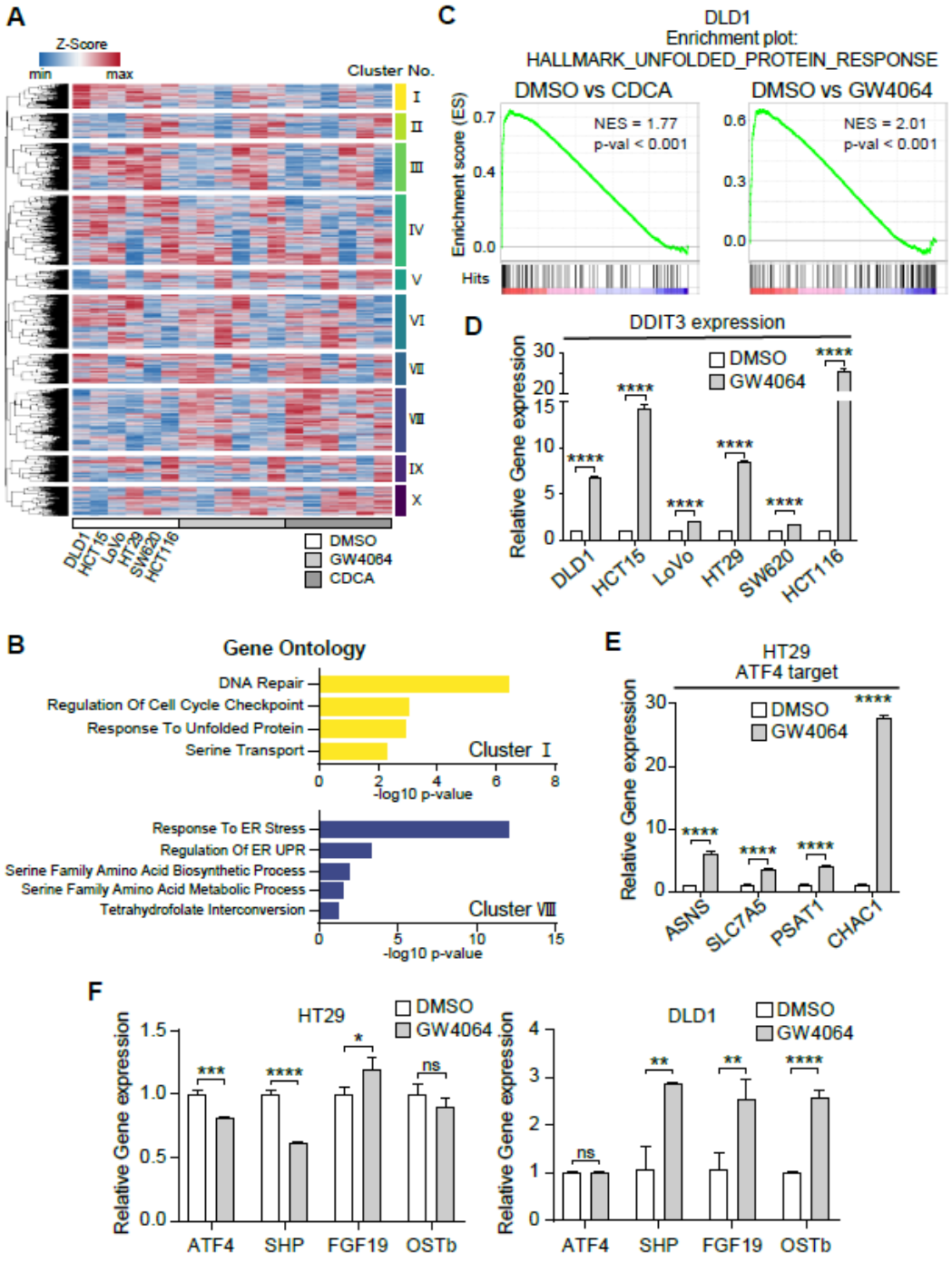

Figure 5. The activation of FXR is indicative of changes in various pathways. (A) Heatmap of CRC cell lines mRNA-seq treated FXR agonists (GW4064, CDCA). (B) GO analysis of mRNA-seq clusters. Bar charts displaying the GO terms for biological process. (C) GSEA plots show gene enrichment pattern of unfolded protein response was increased at FXR agonists. (D-E) Bar graphs show mRNA levels of DDIT3 and ATF4 target genes in colorectal cancer cell lines and HT29. (F) Bar graphs show mRNA levels of ATF4 and FXR target genes in colorectal cancer cell lines (HT29 and DLD1). Data represent mean + SEM. *p<0.05, **p<0.01, ***p<0.001, ****p<0.0001; student's t-test, two tailed.

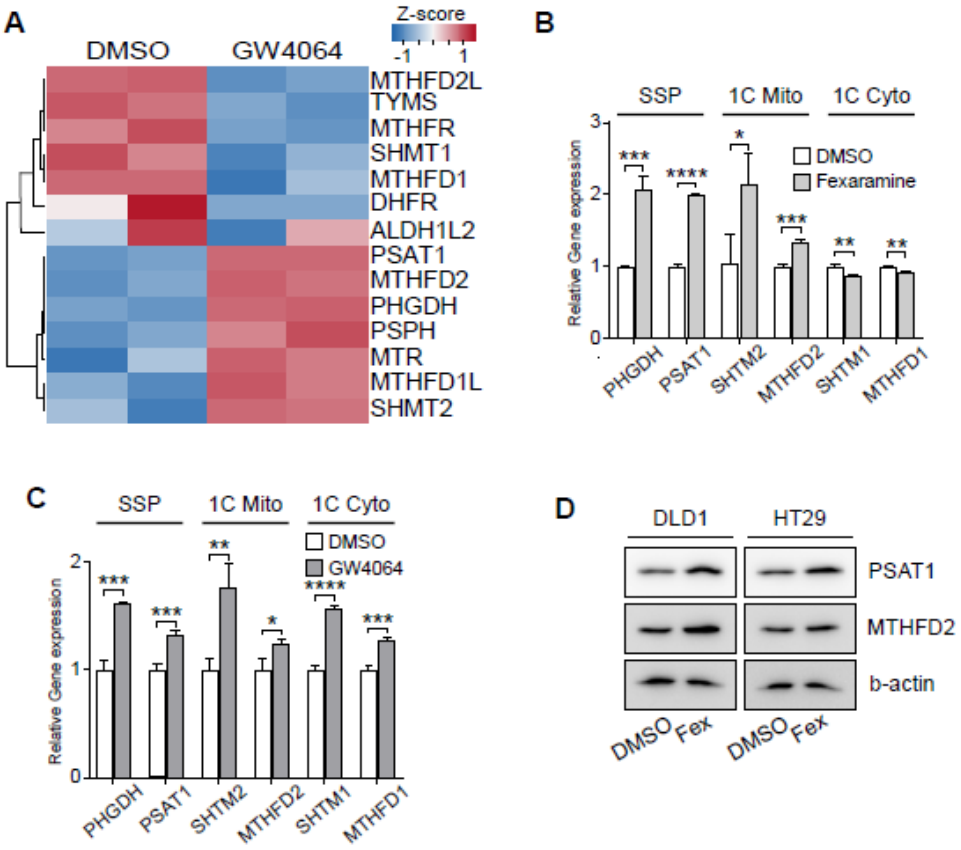

Figure 6. One-carbon metabolism increases as a compensatory pathway in response to FXR activation. (A) Heatmap showing the expression levels of one-carbon metabolism genes in mRNA-seq. (B-C) Bar graphs show mRNA levels of one-carbon metabolism genes in HT29 treated with Fexaramine and GW4064. (D) Western blot displays PSAT1, MTHFD2, and β-actin treated with fexaramine for 24h. Data represent mean + SEM. *p<0.05, **p<0.01, ***p<0.001, ****p<0.0001; student's t-test, two tailed.

3.5. Single-nucleus transcriptome analysis reveals high one-carbon metabolism signature score with FXR activation

Next, I conducted single-nucleus RNA sequencing (snRNA-seq) analysis of CRC organoids treated with an FXR agonist (Fig. 7A). By applying unbiased clustering to the cells, I identified nine distinct clusters based on competitive GSEA as follows : the E2F pathway cluster highly expressed CDK1, E2F7, BRCA1, and BRCA2; the hypoxia pathway cluster highly expressed HIF1A, NDRG1, and VEGFA; the OXPHOS pathway cluster highly expressed PDHB, SLC25A4, and LGR5; the MYC pathway cluster highly expressed MYC, DDX18, and GNL3; the WNT/beta-catenin pathway highly expressed ZNRF3 and AXIN2; and the NFkB pathway cluster highly expressed GADD45B and TRIB1. The expression profiles of the elected genes in the cell populations are shown (Fig. 7B-D). I determined the specific gene expression pattern for CRC compared with the activation of the FXR. The biological process gene ontologies (GO:BP) enriched in the E2F cluster included one-carbon metabolism processes and response to reactive oxygen species (ROS). One-carbon metabolism gene expression was higher in the E2F cluster than in the other clusters (Fig. 7E, F). Subsequently, I analyzed the CRC organoid data using RNA velocity (scvelo), a computational approach that uses the ratio of spliced to unspliced transcripts to determine whether genes were actively upregulated or downregulated in individual cells. I then conducted a trajectory analysis of the CRC organoid and cell line data using the slingshot algorithm, which is a popular tool for analyzing bifurcation trajectories (Fig. 8A, B). This trajectory suggests that a branch of both datasets could enter the one-carbon metabolism pathway during increased FXR activity and tumorigenesis. I observed an increase in the expression of one-carbon metabolism genes along this trajectory (Fig. 8C). I also observed the expression of several one-carbon metabolism marker genes only in the E2F pathway cluster subset (Fig. 8D, E). Moreover, I confirmed that the CRC cell line single-cell public data had increased one-carbon metabolism pathway activity (Fig. 9A-E). Therefore, the activation of FXR in organoid is expected to induce a one-carbon metabolism, which may function as a survival pathway, similar to the CRC cell data.

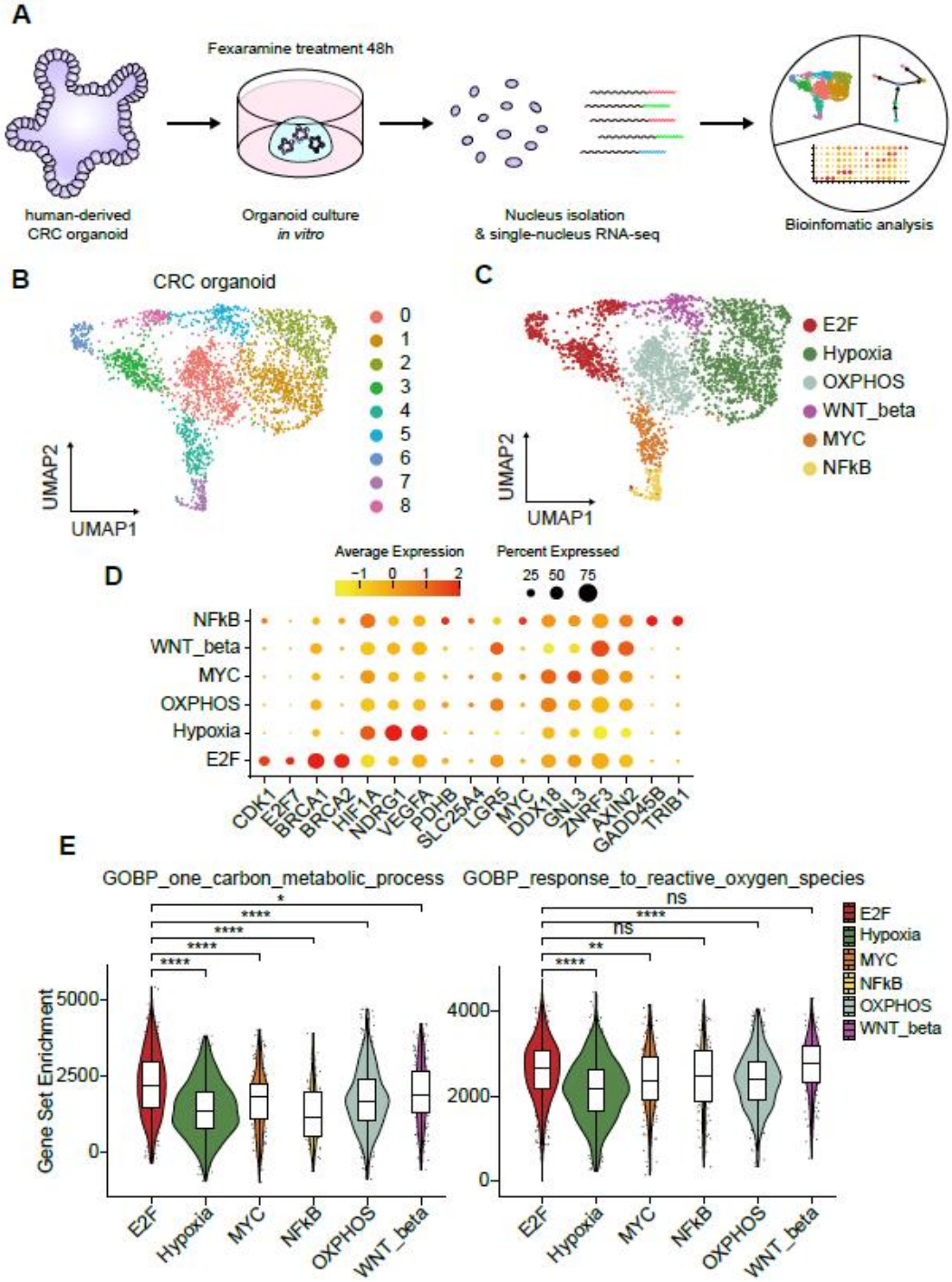

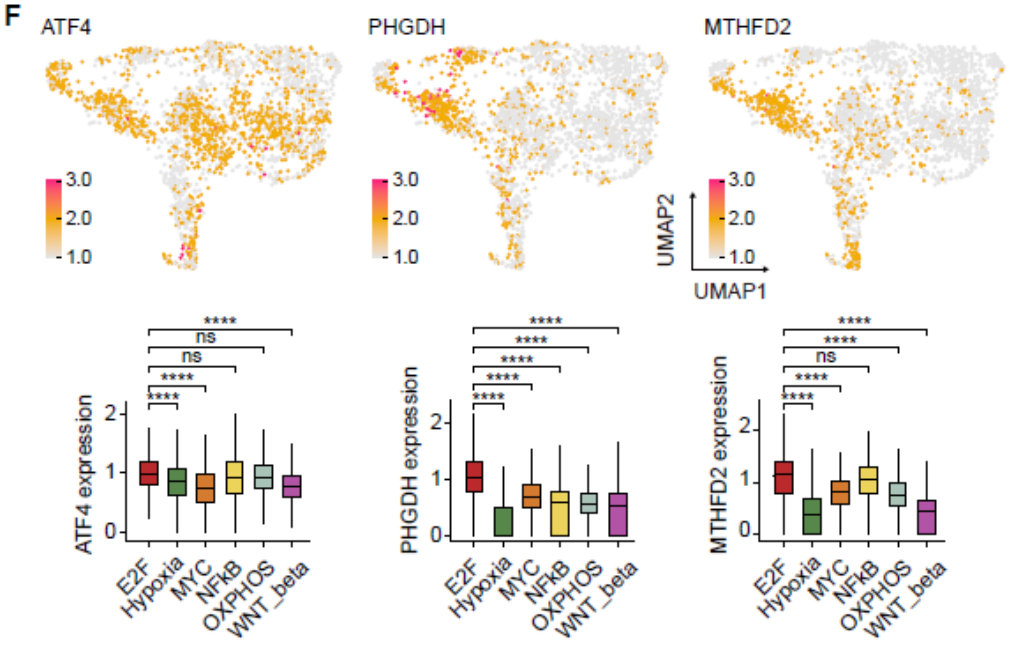

Figure 7. One of the clusters in organoids has high one-carbon metabolism. (A) Schematic diagram illustrating the generation of cDNA libraries and subsequent bioinformatics analyses. (B) UMAP visualization of single nuclei from an organoid in integrated control(DMSO) and fexaramine. (C) UMAP visualization of all cells in organoids. Labeled cell types are the predominant cell types in each cluster. (D) Dot plot displaying the expression of the most highly marker genes of major cell types. (E) The violin plot shows the distribution of enrichment scores for enriched GO pathways derived from upregulated genes in pairwise comparisons among the six groups. Each group is color-coded, with each dot representing a cell. The box plot displays the mean value of the enrichment scores for each pathway. (F) UMAP plots of the normalized expression of 1C marker genes, and Box plot showing 1C marker genes expression. *p<0.05, **p<0.01, ***p<0.001, ****p<0.0001; student's t-test, two tailed; one-way ANOVA followed by TurkeyHSD.

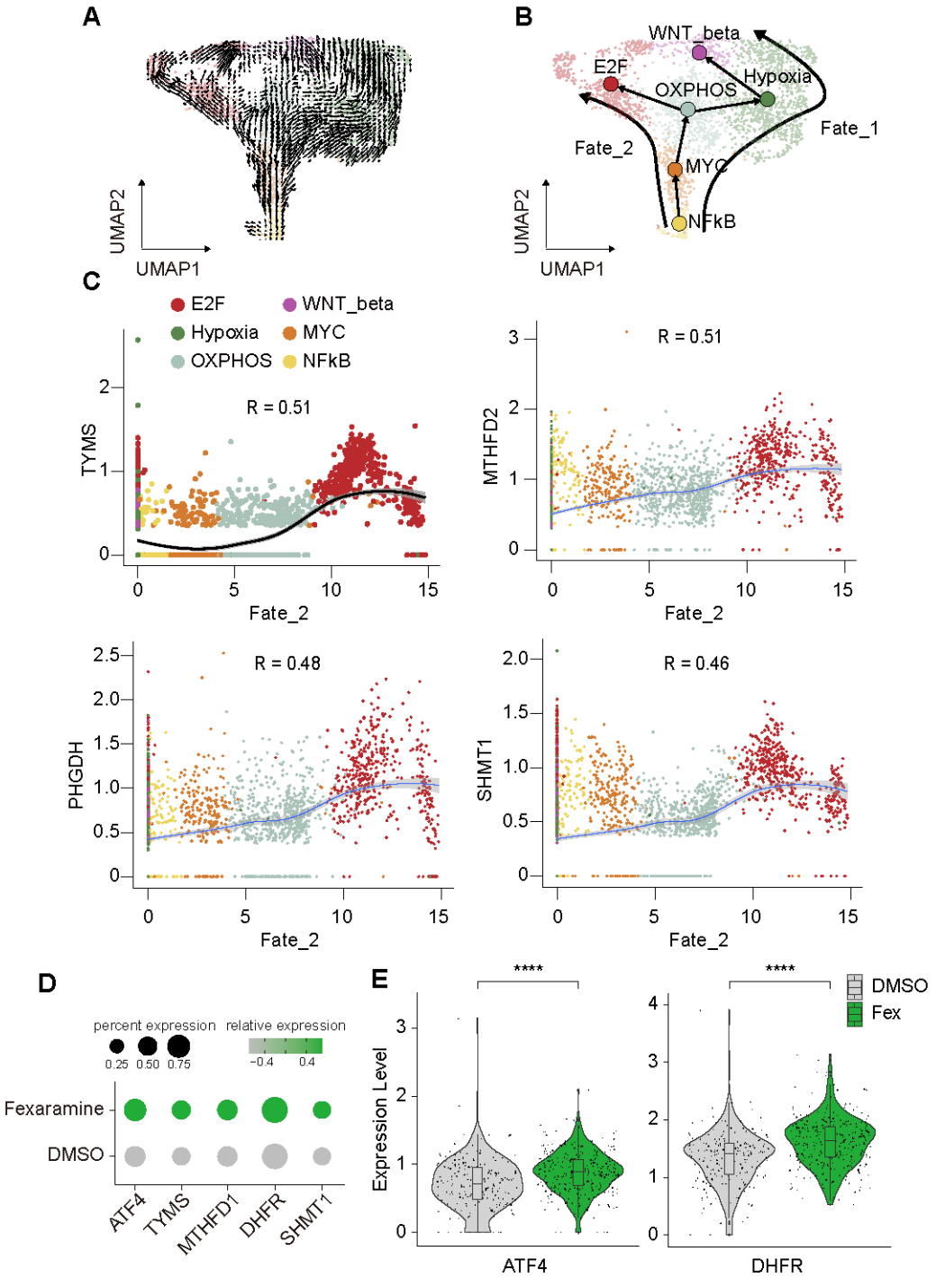

Figure 8. In organoids, the activation of FXR leads to an increase in one-carbon metabolism. (A) Streamlines in a UMAP visualize single-cell velocities for the six clusters, with black arrows indicating the direction along the cell development trajectory. (B) Slingshot-based pseudo-time trajectories were calculated from UMAP. Each trajectory starts from a single point and splits into two endpoints. These trajectories were then plotted together, resulting in a branching appearance. (C) Scatterplot represents a positive correlation between average expression level of TYMS, MTHFD2, PHGDH, SHMT1 (y axis) and pseudotime (x axis) in the CRC organoid. (D-E) Dot plot and violin plot display expression level of 1C metabolism genes between control (DMSO) and fexaramine. *p<0.05, **p<0.01, ***p<0.001, ****p<0.0001; student's t-test, two tailed.

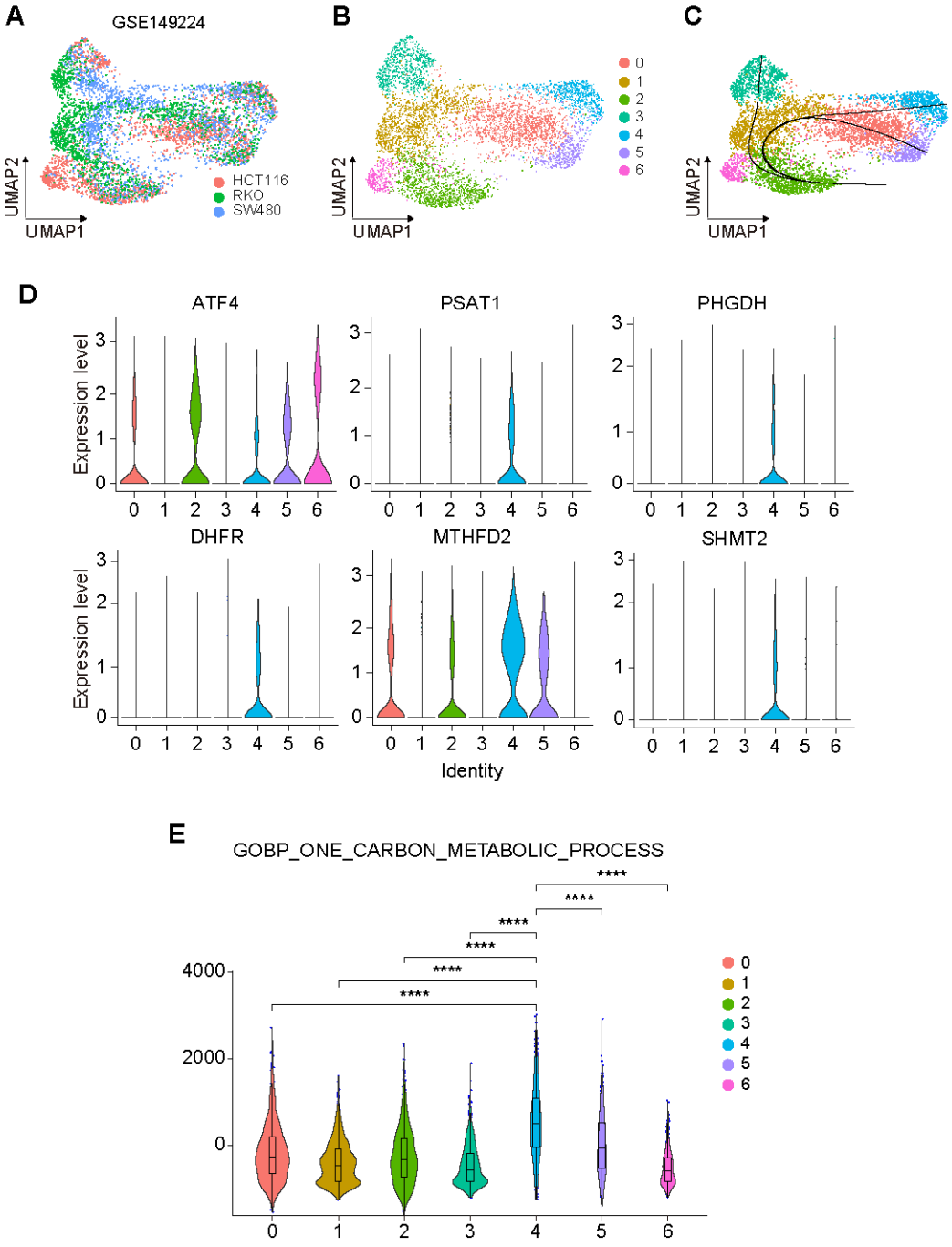

Figure 9. In single-cell sequencing, as in organoids, there is a cluster with elevated one-carbon metabolism. (A-B) UMAP visualization of single cell from integrated HCT116, RKO, SW480 and cluster dividing. The GEO dataset of CRC cell lines are from GSE149224. (C) Slingshot-based pseudo-time trajectories were calculated from UMAP. Each trajectory starts from a single point and splits into two endpoints. These trajectories were then plotted together, resulting in a branching appearance. (D) Violin plot showing 1C marker genes expression. (E) Violin plot distribution of enrichment scores for enriched GO pathways from upregulated genes from pairwise comparison between the seven groups; seven groups are color-coded, each dot represents a cell and the box plot displays the mean value of the enrichment score of each given pathway. *$p<0.05$, **$p<0.01$, ***$p<0.001$, ****$p<0.0001$; student's t-test, two tailed; one-way ANOVA followed by TurkeyHSD.

3.6. Activated FXR binding to ATF4 act as a co-activator to increase ATF4 transcriptional activity

Based on previous results, I was curious to better understand the regulates one-carbon metabolism when FXR was activated. First, I performed an ATF4 downstream pathway gene, DDIT3, promoter luciferase assay. ATF4 transcriptional activity was upregulated by the FXR and the FXR agonist (GW4064) (Fig. 10A). I hypothesized that the FXR functions as a co-activator or enhancer of ATF4 and increases its transcriptional activity. To validate this, I conducted chromatin immunoprecipitation assay (ChIP-assay), co-immunoprecipitation (co-IP), and immunocytochemistry (ICC) experiments to confirm the co-localization and binding of ATF4 and the FXR (Fig. 10B-D). The results demonstrated that since no changes in ATF4 levels were observed (Fig. 5F), the increase in one-carbon metabolism expression is not due to elevated ATF4 levels but rather the increased binding of the two transcription factors, along with their co-localization, upon treatment with an FXR agonist.

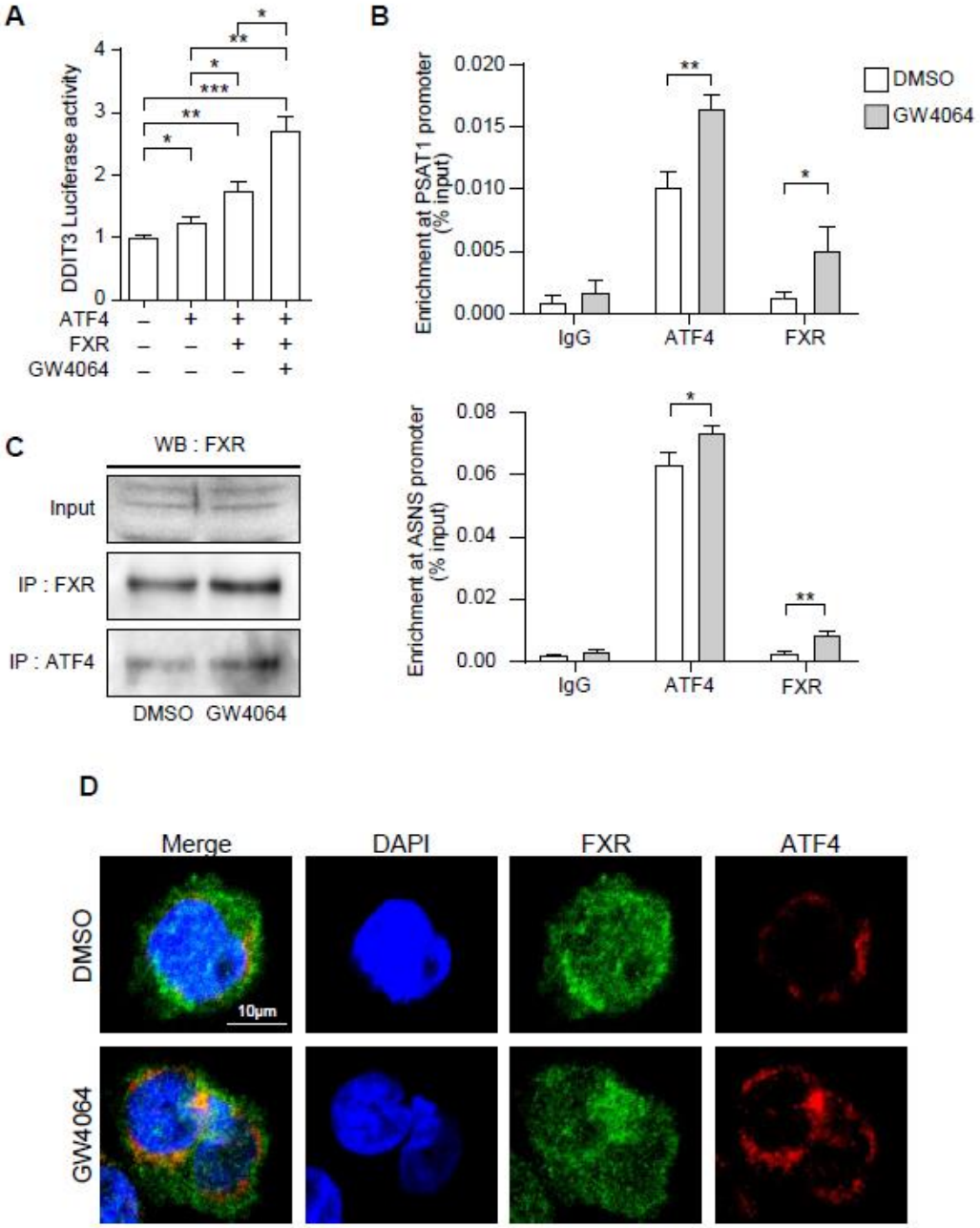

Figure 10. Activated FXR functions by binding with ATF4. (A) The dual luciferase assay for DDIT3 promoter activity in 293T cells that were co-transfected vectors (DDIT3 promoter-luc, β-galatosidase, ATF-GFP, and FXR-Flag vector). Luciferase activities were normalized to the control β-galatosidase values. (B) Quantitative PCR results were used to quantify enrichment of ATF4 and FXR at the ASNS and PSAT1 promoter using ChIP assay. (C) Co-immunoprecipitation analysis of ATF4 and FXR interaction using anti-FXR and anti-ATF4 antibody. (D) Representative immunocytochemistry images showing the colocalization of ATF4-FXR structure in the FXR agonist (GW4064). Scale bar = 10 μm. Data represent mean + SEM. *$p<0.05$, **$p<0.01$, ***$p<0.001$, ****$p<0.0001$; student's t-test, two tailed.

3.7. The transcription factor ATF4 is associated with the control of one-carbon genes in CRC

Modulation of transcriptional activity through the binding of specific DNA regions by transcription factors is a crucial aspect of gene expression. However, the regulatory activity of transcription factor binding is influenced by various factors, including cellular context and regulatory mechanisms such as chromatin modifications. To determine chromatin modifications during FXR activation, I conducted an assay for transposase-accessible chromatin by sequencing (ATAC-seq) and chromatin immunoprecipitation sequencing (ChIP-seq) analysis. The total chromatin structures of the open and closed regions were similar. Although the accessibility of the promoter regions was similar, however, the functional elements and motif activities of the activated FXR group displayed increased accessibility to the chromatin structure (Fig. 11A-C). As expected, the activated FXR group (open chromatin regions) showed an enriched ER response and one-carbon metabolic processes (Fig. 11D). Recruitment of ATF4 to the promoter regions of one-carbon metabolism genes significantly increased upon FXR activation. The chromatin structure of the promoter regions of one-carbon metabolism genes also remained unaltered upon FXR activation. However, ChIP-seq analysis revealed a substantial increase in ATF4 recruitment after FXR activation. (Fig. 11E). These findings indicate that FXR activation does not affect chromatin structure; however, it leads to increased recruitment of ATF4 binding to promoter regions.

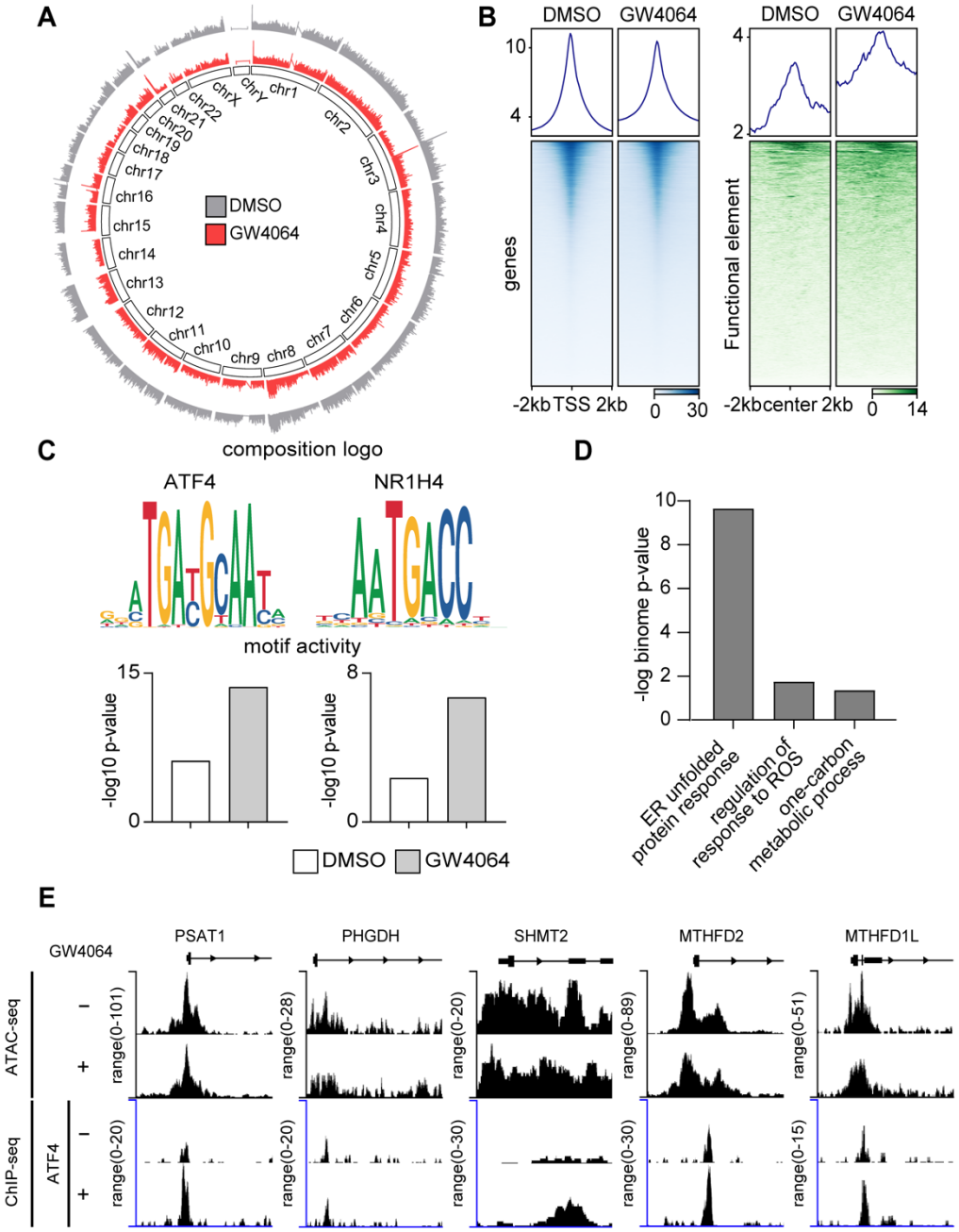

Figure 11. The activation of FXR induces changes in chromatin and increases the recruitment of ATF4. (A) The ShinyCircos graph illustrates the genome-wide chromatin accessibility on chromosomes following a 24 h treatment with the FXR agonist (GW4064). (B Heat map of ATAC-seq peaks based on transcription start site (TSS) and RefSeq functional elements aligned to their center ± 2 kb. (C) The computation of motif activity variability upon FXR agonist treatment was performed using chromVAR. (D) GO analysis shows enrichment of biological processes related to 1C metabolism in FXR agonist treatment cells. The p-value is based on the binominal test. (E) ATF4 ChIP-seq analysis was performed. GBiB shows a comparison of ATAC-seq and ChIP-seq peak signals within the 1C metabolism genes (PSAT1, PHGDH, SHMT2, MTHFD2, and MTHFD1L) loci.

3.8. ATF4 is a crucial regulator of the one-carbon metabolism, which is upregulated by FXR

I verified the correlation between the FXR and ATF4 expression. ATF4, a key transcription factor in the one-carbon metabolism pathway, regulates gene expression. I confirmed its elevated expression in patients with CRC (Fig. 12A). I analyzed TCGA COAD data and demonstrated a positive correlation between ATF4 expression and one-carbon metabolism gene expression. Additionally, I examined the survival curve of the TCGA COAD data which revealed that patients with a high expression of both ATF4 and one-carbon metabolism genes exhibited a poor prognosis (Fig. 12B, C). Furthermore, I speculate that ATF4 plays a crucial role in the response to activated FXR. To confirm this hypothesis, I first silenced ATF4 and found that both the mRNA and protein levels of ATF4 and one-carbon metabolism genes were significantly decreased (Fig. 12D). Second, I found that at the shATF4 RNA sequencing and RNA levels, the expression of ATF4 target genes was downregulated, and that there was also a loss of responsiveness to the FXR agonist (Fig. 12E, F) and decreased levels of ATF4 in its target gene promoter region (Fig. 12G). Additionally, the level and responsiveness of ATF4 decreased when I silenced the FXR (Fig. 12H, I). Taken together, these data demonstrate that in the regulation of one-carbon metabolism genes, the actions of both ATF4 and FXR are required.

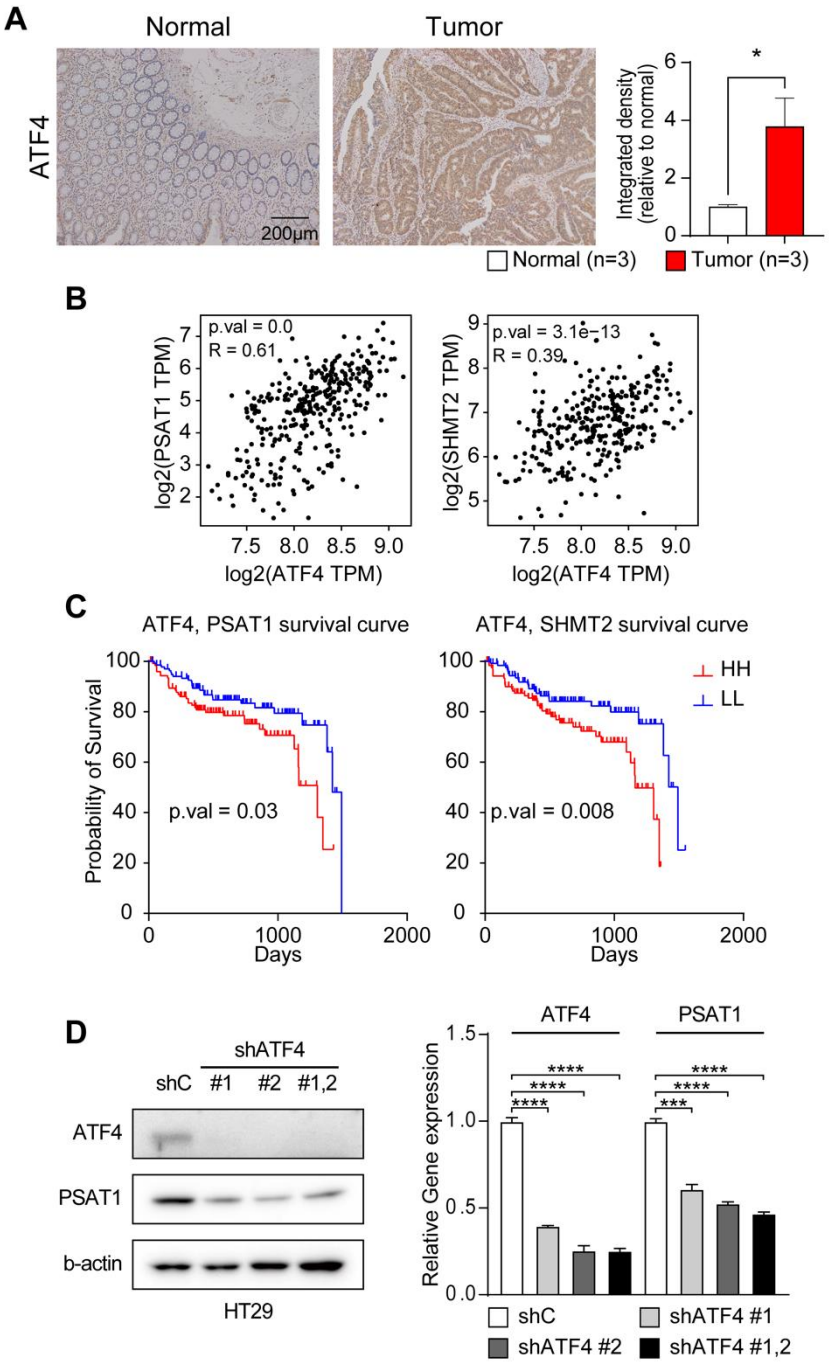

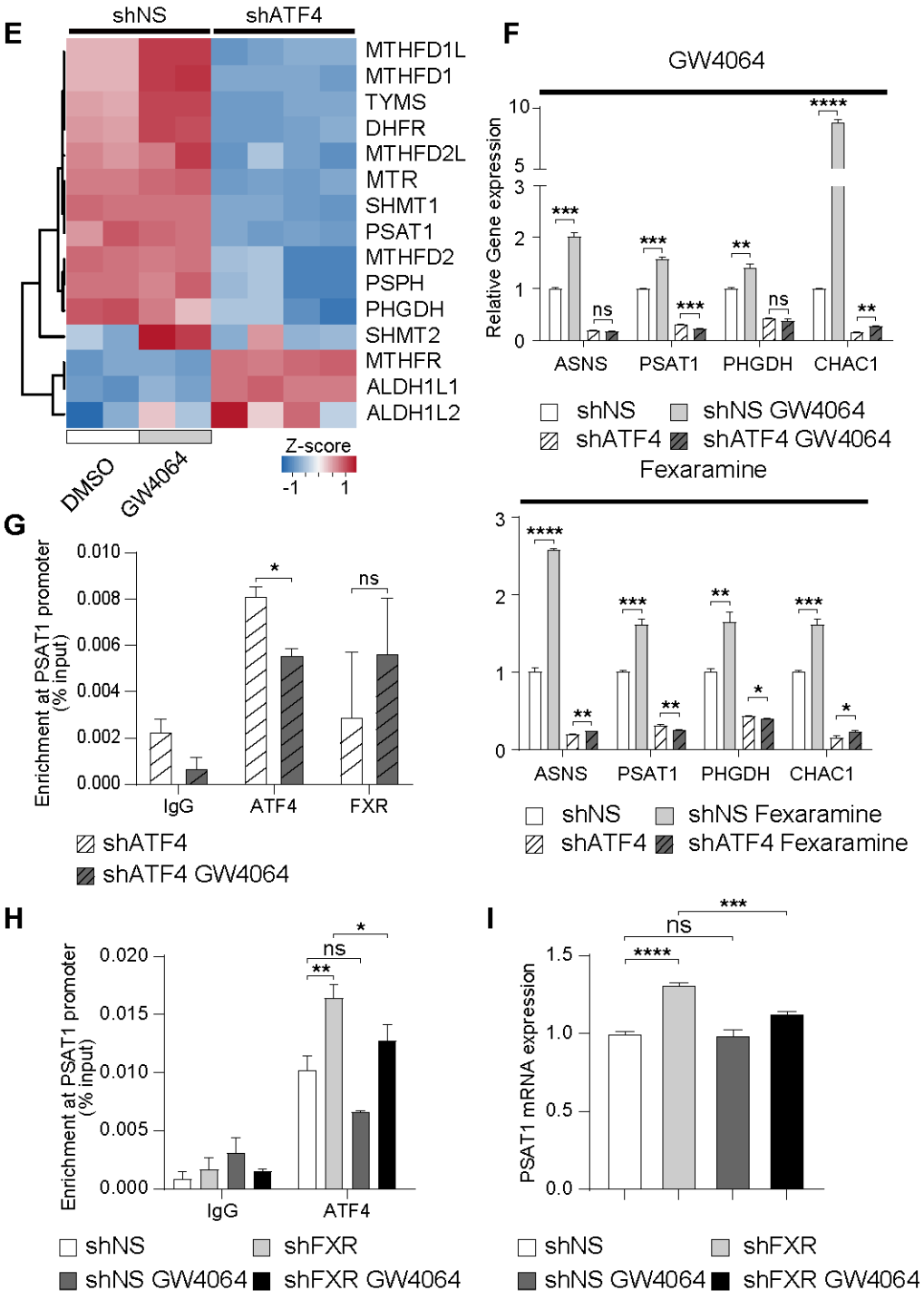

Figure 12. In the regulation of one-carbon metabolism genes, the actions of both ATF4 and FXR are required. (A) IHC staining shows ATF4 expression in patients with CRC. Scale bar = 200 μm. (B) Calculation of Pearson's correlation between various gene expressions was conducted using samples from the GEPIA database. PSAT1 and SHMT2 were positively correlated to ATF4. (C) Kaplan-Meier survival curves show that the group with high expression of ATF4, PSAT1, and SHMT2 had shorter survival among patients with CRC. (D) Western blot shows ATF4, PSAT1, and β-actin protein extract from an ATF4-shRNA cell. Representative quantitative PCR analysis displays ATF4 and PSAT1 mRNA level from an ATF4-shRNA cell. (E) Heat map of the FXR agonist (GW4064) treated ATF4-shRNA cell mRNA-seq. (F) Bar graphs show mRNA levels of ATF4 target genes in ATF4-shRNA cell. (G-H) Quantitative PCR results were used to quantify the enrichment of ATF4 and FXR at the PSAT1 promoter in ATF4-shRNA and FXR-shRNA using ChIP assay. (I) Bar graphs show mRNA levels of PSAT1 in an FXR-shRNA cell. Data represent mean + SEM. *$p<0.05$, **$p<0.01$, ***$p<0.001$, ****$p<0.0001$; student's t-test, two tailed.

3.9. FXR agonist and one-carbon inhibitor combination treatment has a synergistic anti-tumor effect in CRC

My findings suggested that one-carbon metabolism acts as a compensatory pathway in response to FXR activation. The one-carbon metabolism pathway protects cancer cells from growth arrest under various stressful conditions. I examined the effect of co-treatment with an FXR agonist and a one-carbon metabolism pathway inhibitor on cell proliferation. The results showed that the FXR agonist and one-carbon metabolism pathway inhibitor had a synergistic effect on the proliferation of CRC cell lines regardless of the genetic mutations, and this synergistic effect was even observed in human-derived CRC organoids (Fig. 13A). Additionally, the combinatorial treatment of an FXR agonist and a one-carbon metabolism inhibitor appears to have a synergistic effect, as indicated by the HSA score (Fig. 13B). Next, I detected reduced levels of total GSH, which plays a role in determining cellular redox potential, in the combination treatment compared with the treatment with FXR agonists alone (Fig. 13C). GSH synthesis occurs via NADPH production such as during one-carbon metabolism.[23] To identify whether the reduction in total GSH was related to one-carbon metabolism, I examined NADPH production and found that NADPH production levels were also decreased by the combination treatment (Fig. 13D). Because reduced GSH levels lead to an increase in cellular ROS levels, I compared intracellular ROS levels. Combination treatment with FXR activation and one-carbon metabolism pathway inhibition elevated cellular ROS levels, supporting the idea that one-carbon metabolism plays a pivotal role in redox homeostasis (Fig. 13E). Dysfunction of ROS homeostasis by inhibitors leads to the loss of cellular protection against stress, resulting in increased cell cycle arrest and reduced proliferation. Next, a xenograft mouse model was used to assess the effects of FXR activation and inhibition of one-carbon metabolism on tumor growth in vivo. I generated xenograft mouse models by subcutaneously injecting HT-29 cells expressing mCherry into nude mice. Xenograft tumors subjected to combination treatment with an FXR agonist (GW4064) and a one-carbon metabolism inhibitor (NCT-503, SHIN1) exhibited significantly reduced growth rates and smaller sizes compared with those treated with each agent separately. Additionally, the combined treatment results in the xenograft tumors to have a synergistic effect, as indicated by the HSA score (Fig. 13F-H). Moreover, treatment of cancer cells with a combination of FXR agonist and one-carbon metabolism inhibitor resulted in increased apoptotic fragmented nuclei (Fig. 13I). When analyzing through FACS, I observed a shift in the cell population

towards the apoptotic region with annexin V staining, indicating that the combination treatment not only reduced proliferation but also increased apoptosis in cancer cells (Fig. 13J).

My data demonstrated that one-carbon metabolism is a survival pathway against FXR activation and elevating ROS levels through FXR activation and inhibition of one-carbon metabolism is an important phenomenon in the suppression of tumorigenesis (Fig. 14).

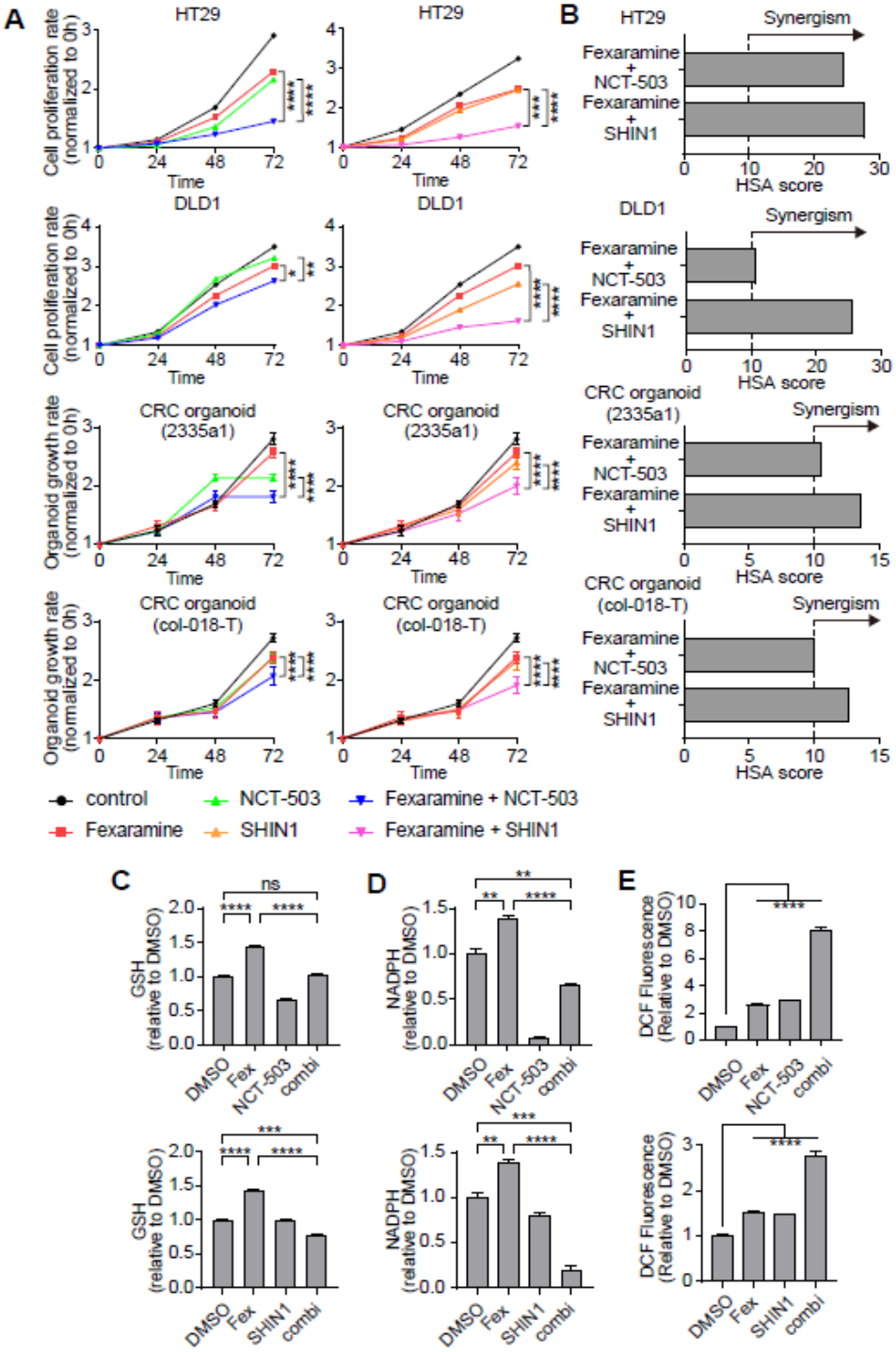

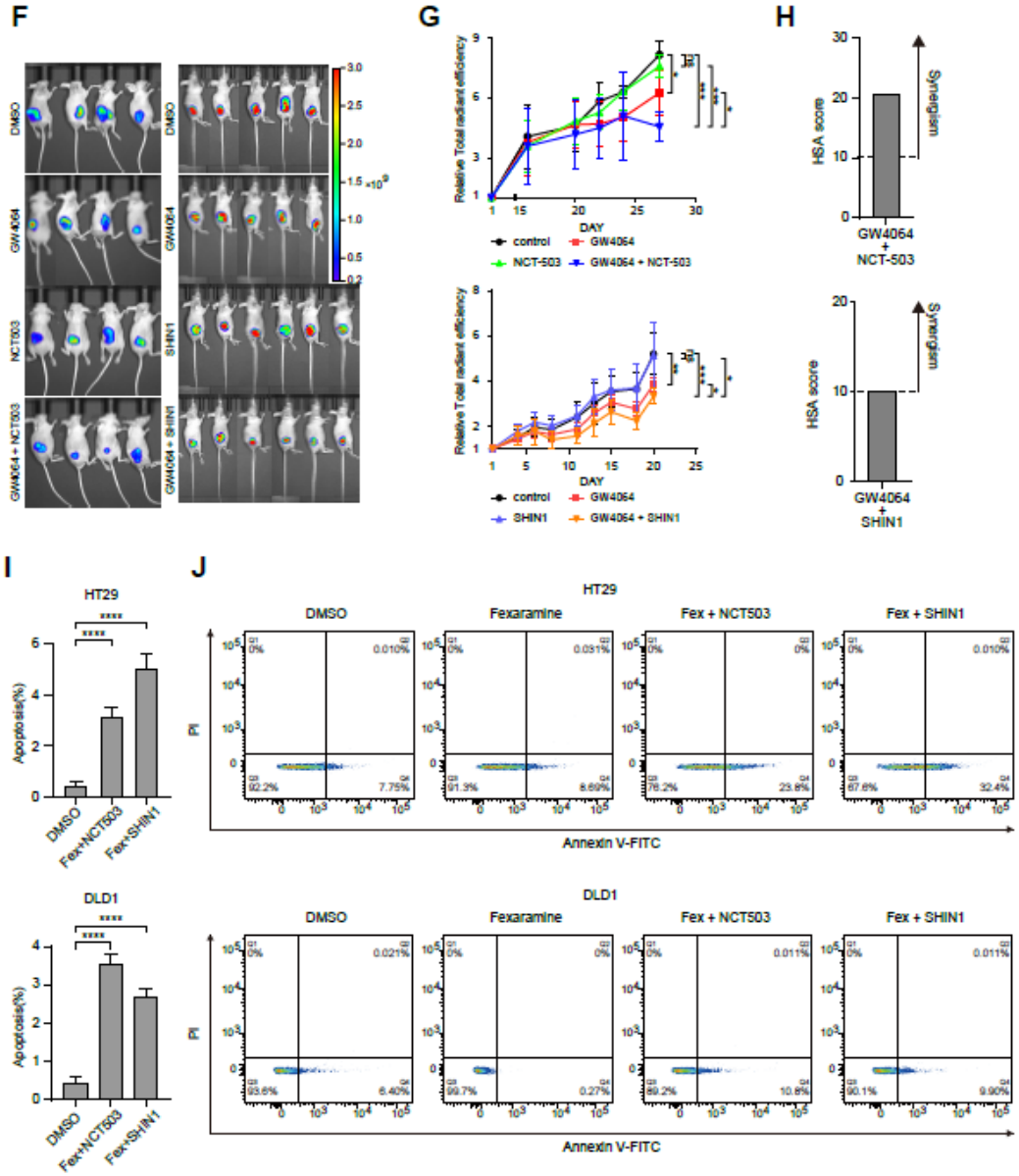

Figure 13. Combination treatment of FXR agonist and one-carbon metabolism inhibitor has a synergistic anti-tumor effect. (A) Cells and organoid underwent treatment with the specified groups (cells : fexaramine; 15 μM, NCT503; 15 μM, SHIN1; 10 μM, organoid : fexaramine; 15 μM, NCT503; 15 μM, SHIN1; 15 μM). Cell proliferation was measured by CCK-8. (B) The synergistic effects of combination treatments were confirmed using the HSA model. (C) The bar graph shows total GSH levels in specified groups by mBBr staining (10 μM) in flow cytometry. (D) The bar graph shows intracellular NADPH levels in specified groups. (E) The bar graph shows intracellular ROS levels in specified groups by H2DCFDA staining (10 μM). (F) A representative image of mice ($n \geq 4$) with tumor volume was obtained using an in vivo optical imaging system. The measurement of total radiant efficiency (p/sec/cm²/sr / μW/cm²) was performed in the tumor area. (G) Total radiant efficiency was compared in every group ($n \geq 4$) until day 20 and 27 after injection (vehicle, GW4064; 20 mg/kg, NCT503; 30 mg/kg, SHIN1; 30mg/kg). (H) The synergistic effects of combination treatments were confirmed using the HSA model in vivo. (I) The bar graph shows quantifying the percentage of fragmented nuclei. (J) FACs results with Annexin V(FITC)/PI staining. Cells were classified as normal cells ($FITC^-$,PI^+), early apoptotic cells ($FITC^+$, PI^-), dead cells ($FITC^+$, PI^+), and damaged cells ($FITC^-$, PI^+) Data represent mean + SD. *p<0.05, **p<0.01, ***p<0.001, ****p<0.0001; student's t-test, two tailed.

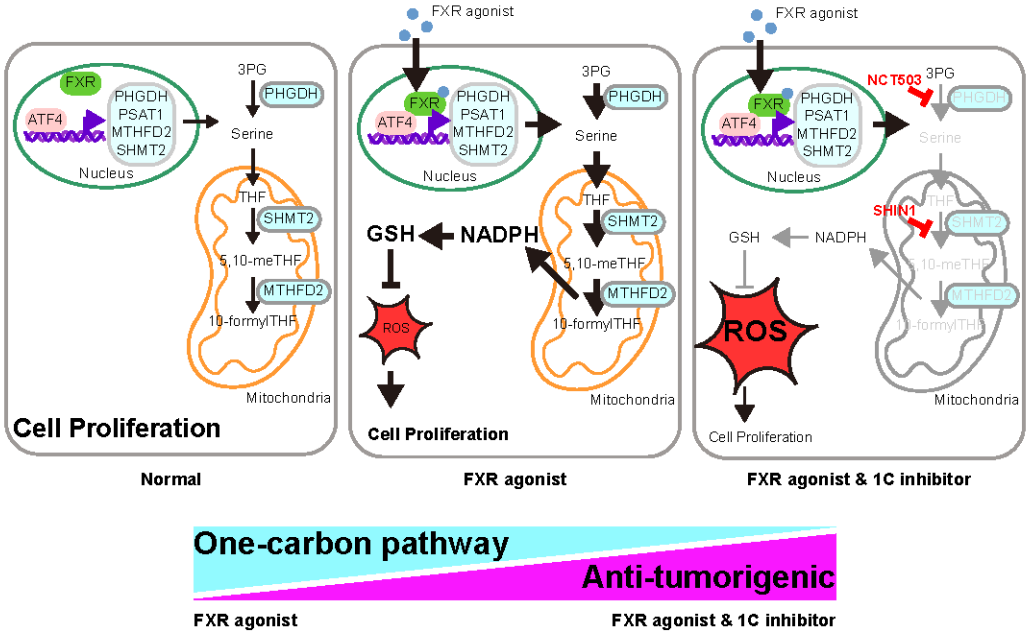

Figure 14. Schematic model of FXR-ATF4-one-carbon metabolism axis mediated cell survival in CRC.

4. DISCUSSION

Recent studies have shown that susceptibility to intestinal tumorigenesis is primarily mediated by the absence of the FXR rather than by elevated levels of bile acids.[9,24] Although the activation of the FXR demonstrates potential as a chemotherapeutic approach, the intricate signaling network and heterogeneity of tumors could impede the development of effective targeted therapies for tumor suppression in patients with CRC.[25,26] According to the results of many studies supporting these data, FXR-deficient mice show increased proliferation and carcinogenesis, and the activation of the FXR reduced proliferation.[15,27] This indicates that the activation of FXR plays a crucial role in cancer suppression. Obeticholic acid (OCA), a newly developed FXR agonist, has been FDA-approved for primary biliary cholangitis treatment.[28] Furthermore, it has demonstrated potential as an antitumor agent against cholangiocarcinoma and HCC.[29,30] Many studies are investigating cancer treatment through the activation of FXR. According to my findings, FXR activation leads to cell cycle arrest and inhibition of cell proliferation. However, despite inhibiting proliferation, cancer cells have been shown to have a survival pathway that remains unclear.

In this study, I demonstrated that the survival pathway of colorectal cancer cells when FXR is activated. I found that the upregulation of the serine biosynthesis pathway and the folate cycle are key adaptations driving the survival pathway activated by FXR in CRC. Noteworthy, the serine biosynthesis pathway and the folate cycle pathway are included in the one-carbon metabolism.

In a recent study, one-carbon metabolism pathway genes such as PHGDH, PSAT1, MTHFD2, and SHMT2 were found to play pivotal roles in CRC metabolism, including ROS. PHGDH is a gene involved in the serine biosynthesis pathway. In addition to catalyzing de novo serine synthesis, it can promote carcinogenesis by producing the tumor metabolite d-2-hydrozyglutarate(d-2HG). Beyond its role in carcinogenesis, PHGDH is also associated with cancer prognosis. High PHGDH expression in CRC tissues is correlated with late-stage CRC and poor survival, and it also functions as a predictor for prognosis in CRC.[31] In addition, high expression levels of PSAT1, MTHFD2, and SHMT2 lead to CRC progression and may serve as prognostic factors.[32,33]

My data also demonstrated that one-carbon metabolism genes, specifically the folate cycle in mitochondria such as SHMT2 and MTHFD2, up-regulated by FXR activation and it serves as possible factors for prognostic of FXR activation resistance in CRC, similar to their role as predictor in various cancers. The main role of one-carbon metabolism is to regulate ROS through redox

homeostasis.[34,35] My study indicated that FXR activation by FXR agonists not only inhibited the proliferative potential of CRC cells but also increased the genes associated with one-carbon metabolism.

In a study on NASH associated with FXR signaling, an elevation in mitochondrial ROS was observed. ROS are produced in response to both internal and external stimuli in cell. Recent evidence indicates that an altered redox balance and deregulated redox signaling, both common hallmarks of cancers, are strongly implicated in malignant progression and treatment resistance. Cancer cells consistently exhibit high levels of ROS. Excessive ROS generation has been implicated in the development of liver diseases, including NASH.[36-39]

Consequently, their mitochondria must enhance their antioxidant capacity to reduce levels of levels and prevent cell death. Crucially, cancer cells need to maintain a steady state level of ROS, or redox balance, to allow for cell proliferation. Thus, ROS levels are tightly regulated in cancer cells. Furthermore, the genetic modification of malignant cells facilitates the persistent and increased generation of ROS. Elevated levels of ROS can stimulate tumor growth and malignant progression.[40,41] Excessive ROS can induce cell death, so one-carbon metabolism is likely elevated in cancer to maintain ROS optimally.

Additionally, since nucleotides are essential for cancer proliferation, one-carbon metabolism is thought to be elevated to support nucleotide synthesis. Upon FXR activation, one-carbon metabolism is expected to increase primarily to manage the elevated ROS induced by the FXR agonist rather than for nucleotide synthesis. My study demonstrated that one-carbon metabolism maintains this ROS and redox balance during FXR activation. Thus, my findings regarding the increased expression of one-carbon metabolism through FXR activation could potentially inform the development of therapeutic strategies for CRC.

FXR, also known as bile acid receptor, is highly expressed in various tissues, including the liver, intestine, colon, kidney, and stomach. The FXR, a ligand-activated transcription factor, can modulate gene expression through DNA binding either as a monomer or in conjunction with RXR as a heterodimer. Furthermore, the FXR regulates a large number of genes involved in various metabolic pathways such as bile acid synthesis, cholesterol homeostasis, lipid metabolism, and glucose metabolism.[13,42-46]

In the present study, ceramide synthesis and levels were induced by intestinal FXR treatment.

Ceramides induce ER and mitochondrial oxidative stress in hepatocytes.[47,48] The mouse model of type 2 diabetes also showed that treatment with an FXR antagonist reduced ER stress by reducing PERK and eIF2α phosphorylation.[49,50] These findings show that the FXR is closely related to stress signaling; however, the underlying mechanism remains unclear.

My data also demonstrated that FXR activation is correlated with survival signaling, which is one-carbon metabolism. Most of the one-carbon metabolism genes regulated by the transcription factor ATF4. However, in this study, my data indicated that ATF4 expression is not affected by FXR activation, confirming that ATF4 levels do not significantly influence the expression of one-carbon metabolism genes. Additionally, ATAC-seq results showed no changes in chromatin structure upon FXR agonist treatment, while ChIP-seq and ChIP-assay results indicated an increase in ATF4 recruitment. This suggests that the changes in one-carbon metabolism gene expression are due to increased activity of the transcription factor rather than changes in chromatin structure. My study revealed that the FXR binds to ATF4, a stress-signaling transcription factor, and acts as a co-activator, resulting in increased transcriptional activity of ATF4.

In recent times, researchers have outlined consensus molecular subtypes (CMS) through a methodical process, seeking to define the genetic and molecular mutations specific to individuals with CRC. CRC can be categorized into four subtypes, each presenting unique molecular, biological, pathological, and genetic features.[22,51] According to my analysis of public data, it has been confirmed that one-carbon metabolism is increased in tumors, regardless of CMS. However, notably, a significant increase was observed, particularly in types 1 to 3. Additionally, approximately 50% of patients with CRC, especially metastatic CRC, exhibit mutated genes such as KRAS and BRAF.[52,53] CRC has also been shown to overexpress the EGFR, which plays a key role in the progression and initiation of CRC.[54] EGFR activation promotes tumor proliferation, invasion, and migration via the RAS-RAF-MAPK and PI3K-AKT-mTOR pathways. These signaling pathways are triggered by KRAS and BRAF.[55,56] In addition, KRAS and BRAF mutations are common and are not only associated with poor overall survival, but are also responsible for resistance to anti-EGFR therapies, such as cetuximab and panitumumab.[57,58]

Interestingly, my results showed that treatment with one-carbon metabolism inhibitor is more effective than treatment with an Elrotinib (EGFR inhibitor), regardless of mutations. Furthermore, the combination treatment of an FXR agonist and a one-carbon metabolism inhibitor showed better

efficacy in CRC with KRAS and BRAF mutations. One-carbon metabolism inhibitor has already demonstrated effectiveness in CRC regardless of mutations. Therefore, one-carbon metabolism could be a potential target for patients resistant to conventional chemotherapy. Additionally, since the combination treatment with existing chemotherapeutic agents has not yet fully explored, further research is needed in this area, which could lead to new therapeutic strategies. Therefore, my novel therapeutic strategy can be used to update the guidelines for patients with CRC.

5. CONCLUSION

In summary, I explored the functions of activated FXR, revealing that its correlation with ATF4 in CRC. My investigation indicates their involvement in the upregulation of a compensatory tumor survival pathway. My findings demonstrate that activated FXR binds to ATF4, acting as a co-activator to enhance the transcriptional regulation of genes in the one-carbon metabolism pathway. Moreover, I emphasize that the one-carbon metabolism pathway plays a crucial role in CRC survival through activating FXR.

REFERENCE

1. World Health Organization. cancer. World Health Organization.
2. O'Keefe SJ. Diet, microorganisms and their metabolites, and colon cancer. Nat Rev Gastroenterol Hepatol 2016;13:691-706.
3. Choi YY, Lee JK, Kim HS, Kim DW, Kim HM, Kang DR. Medications and the Risk of Colorectal Cancer in Patients with Inflammatory Bowel Diseases: Use of the Landmark Method. Yonsei Med J 2021;62:997-1004.
4. Zhang Z, Zhu X. MiR-103a-3p Contributes to the Progression of Colorectal Cancer by Regulating GREM2 Expression. Yonsei Med J 2022;63:520-9.
5. Zhan T, Rindtorff N, Boutros M. Wnt signaling in cancer. Oncogene 2017;36:1461-73.
6. Zhao H, Ming T, Tang S, Ren S, Yang H, Liu M, et al. Wnt signaling in colorectal cancer: Pathogenic role and therapeutic target. Molecular cancer 2022;21:144.
7. Jeong W-J, Ro EJ, Choi K-Y. Interaction between Wnt/β-catenin and RAS-ERK pathways and an anti-cancer strategy via degradations of β-catenin and RAS by targeting the Wnt/β-catenin pathway. NPJ Precision oncology 2018;2:5.
8. Debruyne PR, Bruyneel EA, Karaguni IM, Li X, Flatau G, Müller O, et al. Bile acids stimulate invasion and haptotaxis in human colorectal cancer cells through activation of multiple oncogenic signaling pathways. Oncogene 2002;21:6740-50.
9. Degirolamo C, Modica S, Palasciano G, Moschetta A. Bile acids and colon cancer: Solving the puzzle with nuclear receptors. Trends Mol Med 2011;17:564-72.
10. Lipkin M, Reddy B, Newmark H, Lamprecht SA. Dietary factors in human colorectal cancer. Annu Rev Nutr 1999;19:545-86.
11. Nguyen TT, Ung TT, Kim NH, Jung YD. Role of bile acids in colon carcinogenesis. World J Clin Cases 2018;6:577-88.
12. Lee FY, Lee H, Hubbert ML, Edwards PA, Zhang Y. FXR, a multipurpose nuclear receptor. Trends Biochem Sci 2006;31:572-80.
13. Wang YD, Chen WD, Moore DD, Huang W. FXR: a metabolic regulator and cell protector. Cell Res 2008;18:1087-95.
14. Sun L, Cai J, Gonzalez FJ. The role of farnesoid X receptor in metabolic diseases, and gastrointestinal and liver cancer. Nat Rev Gastroenterol Hepatol 2021;18:335-47.
15. Fu T, Coulter S, Yoshihara E, Oh TG, Fang S, Cayabyab F, et al. FXR Regulates Intestinal

Cancer Stem Cell Proliferation. Cell 2019;176:1098-112.e18.

16. Modica S, Murzilli S, Salvatore L, Schmidt DR, Moschetta A. Nuclear bile acid receptor FXR protects against intestinal tumorigenesis. Cancer Res 2008;68:9589-94.
17. Yin Y, Wang M, Gu W, Chen L. Intestine-specific FXR agonists as potential therapeutic agents for colorectal cancer. Biochem Pharmacol 2021;186:114430.
18. Ducker GS, Rabinowitz JD. One-Carbon Metabolism in Health and Disease. Cell Metab 2017;25:27-42.
19. Pan S, Fan M, Liu Z, Li X, Wang H. Serine, glycine and one-carbon metabolism in cancer (Review). Int J Oncol 2021;58:158-70.
20. Pranzini E, Pardella E, Muccillo L, Leo A, Nesi I, Santi A, et al. SHMT2-mediated mitochondrial serine metabolism drives 5-FU resistance by fueling nucleotide biosynthesis. Cell Rep 2022;40:111233.
21. Peng Z, Ye M, Ding H, Feng Z, Hu K. Spatial transcriptomics atlas reveals the crosstalk between cancer-associated fibroblasts and tumor microenvironment components in colorectal cancer. J Transl Med 2022;20:302.
22. Guinney J, Dienstmann R, Wang X, de Reyniès A, Schlicker A, Soneson C, et al. The consensus molecular subtypes of colorectal cancer. Nat Med 2015;21:1350-6.
23. Konno M, Asai A, Kawamoto K, Nishida N, Satoh T, Doki Y, et al. The one-carbon metabolism pathway highlights therapeutic targets for gastrointestinal cancer (Review). Int J Oncol 2017;50:1057-63.
24. Guofeng Xie J-PR. The farnesoid X receptor and colon cancer. Journal of Cancer Metastasis and Treatment 2016;2.
25. Gerhards NM, Rottenberg S. New tools for old drugs: Functional genetic screens to optimize current chemotherapy. Drug Resist Updat 2018;36:30-46.
26. Thompson MD, Moghe A, Cornuet P, Marino R, Tian J, Wang P, et al. β-Catenin regulation of farnesoid X receptor signaling and bile acid metabolism during murine cholestasis. Hepatology 2018;67:955-71.
27. Maran RR, Thomas A, Roth M, Sheng Z, Esterly N, Pinson D, et al. Farnesoid X receptor deficiency in mice leads to increased intestinal epithelial cell proliferation and tumor development. J Pharmacol Exp Ther 2009;328:469-77.
28. Markham A, Keam SJ. Obeticholic Acid: First Global Approval. Drugs 2016;76:1221-6.

29. Ali AH, Lindor KD. Obeticholic acid for the treatment of primary biliary cholangitis. Expert Opin Pharmacother 2016;17:1809-15.
30. Yu J, Yang K, Zheng J, Zhao W, Sun X. Synergistic tumor inhibition of colon cancer cells by nitazoxanide and obeticholic acid, a farnesoid X receptor ligand. Cancer Gene Ther 2021;28:590-601.
31. Jia XQ, Zhang S, Zhu HJ, Wang W, Zhu JH, Wang XD, et al. Increased Expression of PHGDH and Prognostic Significance in Colorectal Cancer. Transl Oncol 2016;9:191-6.
32. Qian C, Xia Y, Ren Y, Yin Y, Deng A. Identification and validation of PSAT1 as a potential prognostic factor for predicting clinical outcomes in patients with colorectal carcinoma. Oncol Lett 2017;14:8014-20.
33. Chen J, Na R, Xiao C, Wang X, Wang Y, Yan D, et al. The loss of SHMT2 mediates 5-fluorouracil chemoresistance in colorectal cancer by upregulating autophagy. Oncogene 2021;40:3974-88.
34. Hong T, Chen Y, Li X, Lu Y. The Role and Mechanism of Oxidative Stress and Nuclear Receptors in the Development of NAFLD. Oxid Med Cell Longev 2021;2021:6889533.
35. Léveillé M, Estall JL. Mitochondrial Dysfunction in the Transition from NASH to HCC. Metabolites 2019;9.
36. Mudaliar S, Henry RR, Sanyal AJ, Morrow L, Marschall HU, Kipnes M, et al. Efficacy and safety of the farnesoid X receptor agonist obeticholic acid in patients with type 2 diabetes and nonalcoholic fatty liver disease. Gastroenterology 2013;145:574-82.e1.
37. Yoon IC, Eun JR. Pharmacologic therapy for nonalcoholic steatohepatitis focusing on pathophysiology. Yeungnam Univ J Med 2019;36:67-77.
38. Panieri E, Santoro MM. ROS homeostasis and metabolism: a dangerous liason in cancer cells. Cell Death Dis 2016;7:e2253.
39. Fuchs-Tarlovsky V. Role of antioxidants in cancer therapy. Nutrition 2013;29:15-21.
40. Jiang L, Zhang H, Xiao D, Wei H, Chen Y. Farnesoid X receptor (FXR): Structures and ligands. Comput Struct Biotechnol J 2021;19:2148-59.
41. Wang H, Chen J, Hollister K, Sowers LC, Forman BM. Endogenous bile acids are ligands for the nuclear receptor FXR/BAR. Mol Cell 1999;3:543-53.
42. Girisa S, Henamayee S, Parama D, Rana V, Dutta U, Kunnumakkara AB. Targeting Farnesoid X receptor (FXR) for developing novel therapeutics against cancer. Mol Biomed

2021;2:21.

43. Han CY. Update on FXR Biology: Promising Therapeutic Target? Int J Mol Sci 2018;19.
44. Teodoro JS, Rolo AP, Palmeira CM. Hepatic FXR: key regulator of whole-body energy metabolism. Trends Endocrinol Metab 2011;22:458-66.
45. Xie C, Jiang C, Shi J, Gao X, Sun D, Sun L, et al. An Intestinal Farnesoid X Receptor-Ceramide Signaling Axis Modulates Hepatic Gluconeogenesis in Mice. Diabetes 2017;66:613-26.
46. Gonzalez FJ, Jiang C, Patterson AD. An Intestinal Microbiota-Farnesoid X Receptor Axis Modulates Metabolic Disease. Gastroenterology 2016;151:845-59.
47. Chiang JYL, Ferrell JM. Bile acid receptors FXR and TGR5 signaling in fatty liver diseases and therapy. Am J Physiol Gastrointest Liver Physiol 2020;318:G554-g73.
48. Ozcan U, Yilmaz E, Ozcan L, Furuhashi M, Vaillancourt E, Smith RO, et al. Chemical chaperones reduce ER stress and restore glucose homeostasis in a mouse model of type 2 diabetes. Science 2006;313:1137-40.
49. Rahman S, Garrel S, Gerber M, Maitra R, Goel S. Therapeutic Targets of KRAS in Colorectal Cancer. Cancers (Basel) 2021;13.
50. Tol J, Nagtegaal ID, Punt CJ. BRAF mutation in metastatic colorectal cancer. New England Journal of Medicine 2009;361:98-9.
51. Rejali L, Seifollahi Asl R, Sanjabi F, Fatemi N, Asadzadeh Aghdaei H, Saeedi Niasar M, et al. Principles of Molecular Utility for CMS Classification in Colorectal Cancer Management. Cancers 2023;15:2746.
52. Markman B, Javier Ramos F, Capdevila J, Tabernero J. EGFR and KRAS in colorectal cancer. Adv Clin Chem 2010;51:71-119.
53. Therkildsen C, Bergmann TK, Henrichsen-Schnack T, Ladelund S, Nilbert M. The predictive value of KRAS, NRAS, BRAF, PIK3CA and PTEN for anti-EGFR treatment in metastatic colorectal cancer: A systematic review and meta-analysis. Acta Oncol 2014;53:852-64.
54. Midthun L, Shaheen S, Deisch J, Senthil M, Tsai J, Hsueh CT. Concomitant KRAS and BRAF mutations in colorectal cancer. J Gastrointest Oncol 2019;10:577-81.
55. Garcia-Carbonero N, Martinez-Useros J, Li W, Orta A, Perez N, Carames C, et al. KRAS and BRAF Mutations as Prognostic and Predictive Biomarkers for Standard Chemotherapy

Response in Metastatic Colorectal Cancer: A Single Institutional Study. Cells 2020;9.

56. Lièvre A, Bachet JB, Le Corre D, Boige V, Landi B, Emile JF, et al. KRAS mutation status is predictive of response to cetuximab therapy in colorectal cancer. Cancer Res 2006;66:3992-5.

57. van Brummelen EMJ, de Boer A, Beijnen JH, Schellens JHM. BRAF Mutations as Predictive Biomarker for Response to Anti-EGFR Monoclonal Antibodies. Oncologist 2017;22:864-72.

58. Malka D, Rotolo F, Boige V. First-line treatment in metastatic colorectal cancer: Important or crucial? Eur J Cancer 2017;84:363-6.

Abstract in Korean

담즙산 핵 수용체 FXR과 단일탄소대사경로 조절에 따른 새로운 대장암 치료전략개발

대장암은 세계적으로 발병율이 높고 예후가 좋지 않은 종양 중 하나이다. 대장암의 원인은 여러가지가 있지만, 여러 연구에 따르면 담즙산의 지속적인 노출이나 투여가 암을 유발한다는 것이 밝혀졌다. 대장암은 핵 수용체인 FXR의 발현과 상관관계가 있는 것으로 나타났다. 대장암에서 FXR이 낮게 발현되는 것이 밝혀져 FXR을 활성화하는 것이 대장암을 치료하는 방법임을 시사한다. 그러나 FXR 활성화는 세포사멸이 아닌 세포증식의 감소를 유도했다. 이를 통해서 나는 FXR이 활성화된 세포가 살아남기 위한 보상적 생존 경로를 가지고 있을 거라는 가설을 세웠다. 이러한 생존 경로를 확인하기 위해 RNA 및 단일 핵 RNA 시퀀싱 데이터 분석을 수행한 결과, FXR 활성화가 단일탄소대사 경로를 증가시킨다는 사실을 발견하였다. FXR이 활성화되면 단일탄소대사 유전자의 전사인자인 ATF4가 활성화되고, 활성화된 FXR이 ATF4와 결합하여 ATF4의 전사 활성이 증가한다는 사실을 발견했다. 다음으로 단일탄소대사의 효과를 확인하기 위해 단일탄소대사를 억제하여 확인했다. 그 결과 FXR의 활성화와 단일탄소대사의 억제가 대장암의 증식 억제에 시너지 효과를 발휘하는 것을 확인하였다. 종합적으로, 모든 결과는 단일탄소대사를 억제하면 대장암에서 FXR이 매개하는 항종양 효과가 증가된다는 것을 보여준다.

핵심되는 말 : 대장암, FXR, 단일탄소대사